CHARACTERIZATION OF THE DELTA PHASE IN THE IRON - ZINC SYSTEM

By

K. T. KEMBAIYAN

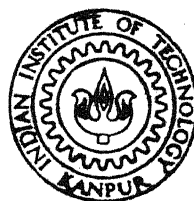**DEPARTMENT OF METALLURGICAL ENGINEERING**

INDIAN INSTITUTE OF TECHNOLOGY, KANPUR

JUNE, 1981

CHARACTERIZATION OF THE DELTA PHASE IN THE IRON - ZINC SYSTEM

A Thesis Submitted
in Partial Fulfilment of the Requirements
for the Degree of
MASTER OF TECHNOLOGY

By

K. T. KEMBAIYAN

to the
DEPARTMENT OF METALLURGICAL ENGINEERING
INDIAN INSTITUTE OF TECHNOLOGY, KANPUR
JUNE, 1981

ME-1981-M-KEM-CHA

CERTIFICATE

29-5-01

Certified that this work on 'Characterization of the δ-phase in the Iron-Zinc System' by Mr. K.T. Kembaiyan has been carried out under my supervision and that this has not been submitted elsewhere for a degree.

(Dr. A.K. Jena)
Professor
Dept. of Metallurgical Engin
Indian Institute of Technolo
Kanpur

ACKNOWLEDGEMENTS

I express my hearty gratitude to Professor A.K. Jena for his excellent guidence and constant advice throughout the course of this work. It was a great pleasure working under the guidence of him and I esteem very much the invaluable experience I gained under his supervision.

I owe to Dr. S.P. Gupta for his assistance in carrying out this work to completion.

I also owe to Dr. Sanjay Gupta, Dr. K.P. Gupta and Dr. D.C. Agarwal for their valuable suggestions and extensive helps. I thank Dr. A. Ghosh for allowing me to use his equipments and Dr. G.K. Mehta for his help in Nuclear Physics Lab.

I am thankful to Mr. A. Sharma of Process Research Lab, Mr. Pandey of X-ray Lab, Mr. Parthwal of A.C.M.S., Mr. Satyaprakash of Nuclear Physics Lab, Mr. Sairam of Glass Blowing Section, Mr. V.P. Gupta of Crystal Growth Lab and to all my friends who helped me at various stages of my work.

Finally my thanks are due to Mr. R.N. Srivastava for typing the manuscript in an elegant form.

- K.T. Kembaiyan

CONTENTS

LIST OF TABLES

LIST OF FIGURES

ABSTRACT

The δ phase of the Fe-Zn system is a major constituent in the galvanized coatings. The durability of the galvanized coating mainly depends on the stability of δ phase but the nature of this phase is not yet very well understood. An attempt has been made in this work to characterize the δ phase by X-ray diffraction and density measurement techniques.

The representative Fe-Zn alloy samples were synthesized by melting the constituent elements in sealed quartz tubes and annealing at different temperatures of interest. The alloys were analysed using Atomic Absorption Spectrophotometer and Proton Induced X-ray Emission Analyser. X-ray diffraction work was carried out on the powders of Fe-Zn alloys and the data on the variation of unit cell parameters of δ phase with composition and heat treatment were obtained. The accurate lattice parameters of δ phase were obtained using the data of previous investigators. Accurate density measurements were carried out on the alloy powders of the δ phase. The X-ray diffraction and density data of the alloys of δ phase indicate a possibility of ordering reaction at about 12.67 at % Fe. It was found that the alloys of 7.68 at % Fe contain both δ and ζ phases, the alloys of 16.01 at % Fe annealed at 605°C and 550°C contain both δ and Γ phases and the alloys of the same composition annealed at 475°C and 350°C contain both δ and Γ_1 phases.

CHAPTER I

INTRODUCTION

A coating of metallic zinc on steel work forms a durable barrier offording good protection of steel work against corrosion under normal conditions. Hot dip galvanizing is the most widely used process for coating metallic zinc over iron. The bonding results in the formation of a number of intermetallic layers of iron-zinc alloys. Unfortunately these phases are not yet very well understood. The stability of many of these phase has been the subject of much dispute.

The major phase present in the galvanized layer is the δ phase and there is a lot of controversy whether this is a single phase or consist of two phases. There seems to be a steep composition change across the δ-phase. During galvanizing, the δ phase in the zinc rich side of the galvanized coat shows lot of cracks whereas the iron rich side of this phase does not show any such cracks. It is reported that this phase has a hexagonal structure consisting of about 550 atoms per unit cell. Thus containing one of the largest unit cell known.

In this project, X-ray diffraction and densitometric investigations of the δ-phase of the iron-zinc system has been carried out so as to get more information on the nature of this phase.

CHAPTER II

REVIEW OF LITERATURE

2.1. Iron-Zinc System :

The equilibrium phase diagram of the Iron-Zinc binary alloy system based on the evaluation of all the data available[1] upto mid 1976 is shown in Figure 2.1. The zinc-rich part of the phase diagram is shown in Figure 2.2. Over the years the phase diagram of Fe-Zn system has undergone constant revision.

The zinc-rich end of the equilibrium phase diagram has received particular attention from the investigators in recent years because of its relevance to hot-dip galvanizing process.

Different forms of the zinc-rich part of the phase diagram has been proposed. One of the oldest was reported by Schramm[2] is shown in Figure 2.3a. Recently a change has been proposed by Ghoniem et al[3] (Figure 2.3b) who distinguishes two different phases in the δ_1 region ($\delta_{1p} + \delta_{1k}$) having different morphologies of the δ_1-layer on galvanized steel. The phase present on the iron-rich side has a compact morphology (δ_{1k}) and on the zinc-rich side a palisade morphology (δ_{1p})

Later in 1977, Bastin et al[4], in his investigations of δ-phase of Fe-Zn system found no evidence in support of
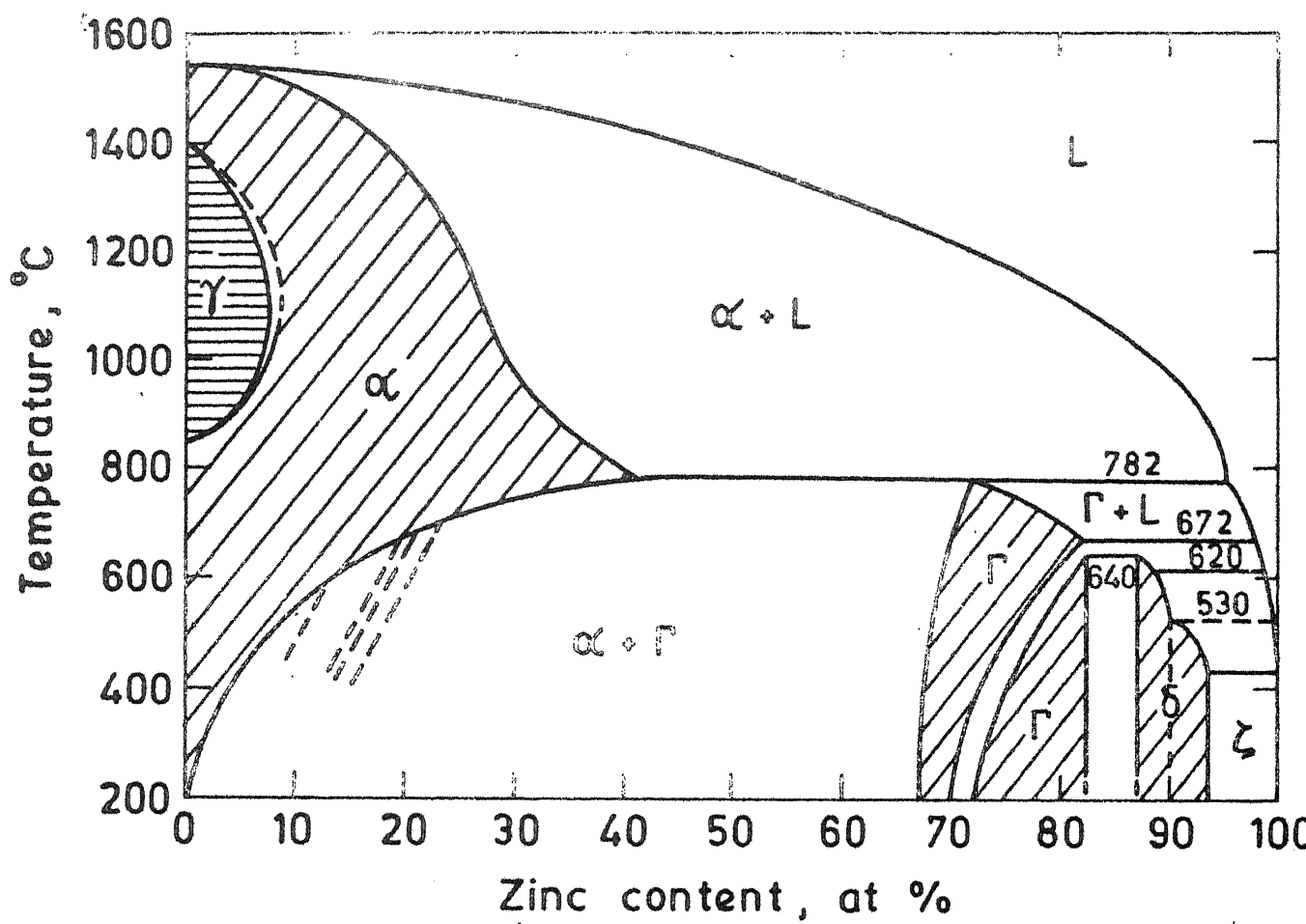
Fig. 2.1. Iron-zinc equilibrium phase diagram.
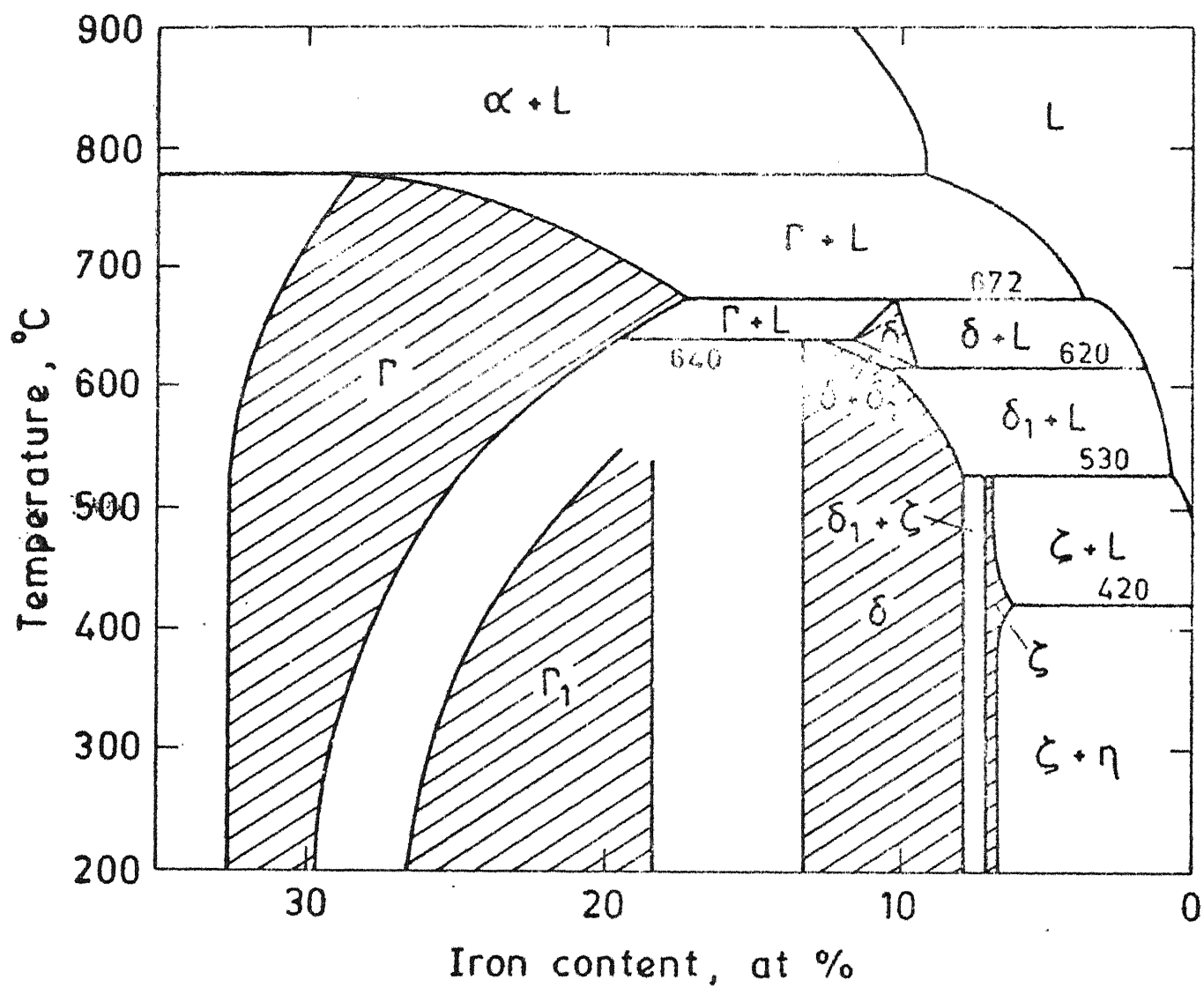
Fig. 2.2. Zinc-rich end of iron-zinc equilibrium phase diagr
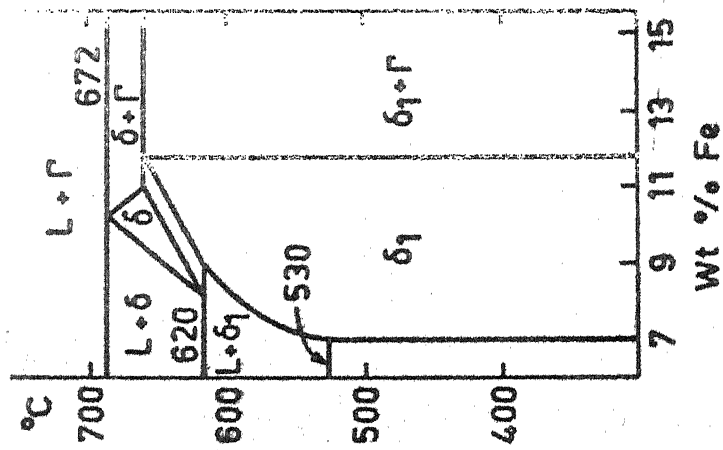
According to Schramm

(a)
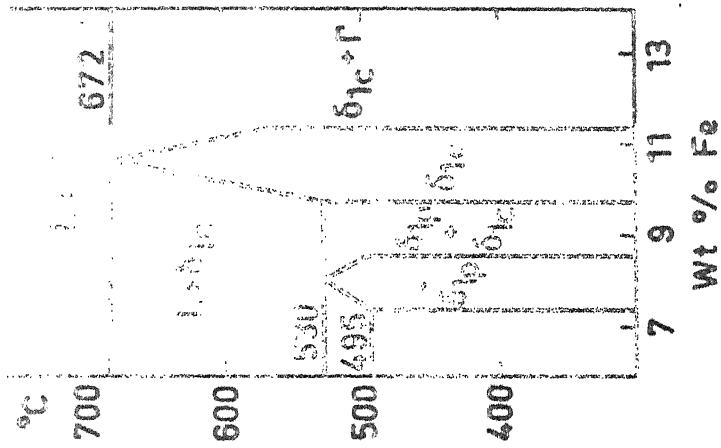
According to Ghoniem & Löhberg

(b)
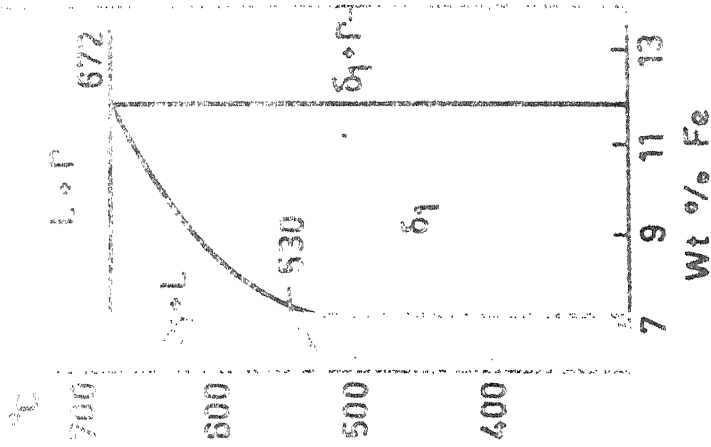
According to Bastin et al

(c)

Fig. 2.3. δ_1 - region of Fe-Zn phase diagram according to various investigators.

the view that the δ phase field would be split up into two
distinct phases δ_p and δ_k as has been suggested by Ghoniem
et al. Bastin proposed a modified phase diagram (Figure
2.3c) for the zinc-rich part of the Fe-Zn system based on
his investigations. This modification by Bastin was found in
close agreement with the results obtained by Gellings[5] and
de Bree in 1978.

2.2. Compounds Present at Different Galvanizing Temperature:

When an iron part is immersed in the molten zinc bath
for galvanizing, as a result of interdiffusion of iron and
zinc atoms, a series of intermetallic Fe-Zn layers are formed.
The nature of the layers present depends on the particular
galvanizing temperature.

At about 490°C, the galvanized coating consists of
a thin Γ-layer adjoining the iron, followed by a thicker
δ_{1k}-layer, a δ_{1p}-layer, a ζ-layer and finally a solidified
η-phase layer.

In the temperature range between 490°C and 520°C,
these alloy layers are partially broken up.

At about 497°C, a very thin Γ-layer is found covering
the iron followed by a thin δ_{1k}-layer and δ_{1p}-layer which
gradually disintegrates towards the melt, followed by large
separated ζ-crystals and solidified η-phase.

Between 497°C and 520°C, the coating consists of a
very thin Γ-layer followed by a thin δ_{1k}-layer, a thin δ_{1p}-
layer and a thick band of δ_1 which has separated from the

coating and is disintegrated to various extents.

At temperatures above 520°C and upto 620°C, the surface layer consists of a thin Γ-layer, a δ_{1k}-layer and a δ_{1p}-layer, the outer portion of δ_{1p} is disintegrated. Between 620°C and 670°C, a layer of Γ is formed next to iron, followed by a layer of angular δ_1 crystals, and finally a mixture of δ_1 and κ.

Above 670°C and upto 782°C, the layer consists of Γ next to the iron and a very thin δ_1-layer which is produced in this temperature by decomposition of the Γ on cooling.

A direct correlation is not always found by relating these observations to the equilibrium phase diagram. The Γ-phase is often missing or not detected. The stability of ζ-phase seems to vary depending on the exact conditions of the treatment. The δ_1 consists of δ_{1k}, δ_{1p} and various forms of disintegrated δ_1-phase. Table 2.1 shows the properties of Fe-Zn intermetallic compounds obtained by different investigators[1].

2.3. Hot-dip Galvanizing:

Zinc coatings are one of the best methods for the protection of steelwork against corrosion since zinc itself is resistant to normal atmospheric corrosion and also it protects the steel parts as a sacrificial anode. Methods of coating includes hot-dip galvanizing, spraying, plating, sherardizing and plating with zinc-containing paints.

Table 2.1. Properties of Fe-Zn Intermetallic Compounds[1].

	Γ, Fe_3Zn_{10}	Γ_1, Fe_5Zn_{21}	δ_1, $FeZn_{10}$	ζ, $FeZn_{13}$
Crystal structure	b.c.c.	f.c.c.	h.c.p.	monoclinic
Lattice parameter, Å	8.97	17.96	a 12.8; c 57.7	a 13.4; b 7.5; c 5.1
Specific gravity	7.36	...	7.24	7.18
Composition range, at.-%				
Hansen and Anderko (450°C)	31.3-23.7	...	13.0-3.1	7.2-6.9
Bastin et al (500°C)	31.5-25.0	21.0-18.5	13.4-8.7	...
Ghoniem & Lohberg (450°C)	...	...	...	7.5-6.5
Onishi et al (s-s at 300°C)	...	...	...	9.5
Short & Mackowiak (s-v at 501°C)	40.2-35.9	24.6-22.1	16.9-12.5	12.2-12.0
Brown (500°C pressure)	...	...	13.4-8.5	7.5-6.7
Microhardness				
Allen	250	...	350-300	200
Bastin et al	326	505	358	208
Drewitt	450	...	380-200	150
Short & Mackowiak (s-v)	265	340	315	250

However, hot-dip galvanizing is most widely used because of its advantages over other processes.

An article to be galvanized is cleaned, pickled and fluxed in a non-continuous process or just heat treated in a reducing atmosphere to remove surface oxide during continuous galvanizing processes. Then it is immersed in a bath of molten zinc for a time sufficient for it to wet and alloy with the zinc, after that it is withdrawn and cooled.

The coating is bonded to the iron by a series of Fe-Zn alloy layers and this is followed by a layer of almost pure zinc. The usefulness and value of the coating depend on the physical and chemical nature of the intermetallic layers formed, and this in turn depends on the particular steel used, the composition of the molten zinc and the conditions prevalent in the bath. The thickest layer formed in the galvanized coating in the δ-layer.

2.4. Kinetics of Growth of Galvanized Coatings :

The nature of the coating and its thickness depends on the time of immersion in the bath, the composition of the bath, and the particular process used. Short immersion times (seconds) are used in continuous processes such as galvanizing sheet, strip or wire and immersion times in the order of a few minutes are used in the case of bath processes for fabricated articles. The thickness of the coating tend to be about 50 μm on thin sections and about

150 μm on thick steel. Most of the commercial galvanizing baths are operated in the temperature range of 450°C and 480°C.

The rates of reaction are expressed mostly by the iron loss method. The growth of the whole and individual layers are determined by metallography or dilatometric methods.

Upto about 490°C, the rate of reaction follows a parabolic law and it is again parabolic above 520°C and in-between those temperatures there is a much enhanced linear attack occurs.

The growth of alloy layers can be expressed by the empirical equation

$$d = ct^n \qquad (2.4.1)$$

where 'd' is the thickness after time 't' and 'c' and 'n' are constants. The rate constant 'c' represents mainly the effect of temperature, and the exponent 'n' characterizes the different growth rates. A value of $n = 1$ indicates a linear rate of growth and a value of $n = 0.5$ indicates a theoretical parabolic rate of growth. The value of 'n' varies for different layers and it has also been found that it may vary with time.

The relative rates of growth for the individual alloy layers in the same surface layer are quite different. The ζ layer grows rapidly at first but then much slowly, while the δ_1 is at first slower than the ζ but then becomes faster and overtakes it. The rate for the Γ-phase is very

slow and therefore this phase may not be seen under the microscope at shorter reaction times.

The thickness of a given phase is determined by the rate of diffusion through the phases which in turn depend on the rates of diffusion in the adjacent phases. Not all the phases will form at the same time, so if diffusion is easier in a phase formed after a delay, it will grow at the expense of the phases formed initially.

2.5. Characteristics of δ Phase:

Ghoniem and Lohberg[3] have studied the δ phase of the Fe-Zn system and observed a concentration jump and a discontinuity in the microhardness[7,8] values at the δ_k/δ_p interface. Hershman[9] has observed the difference in diffusion behaviour in both the δ_k and δ_p layers that the layers were differently attacked by liquid zinc. X-ray diffraction investigations carried out by Bastin et al[10], however, failed to reveal any significant differences in the patterns of the δ phase through the whole concentration range which would comprise both δ_k and δ_p.

Figure 2.4a shows the concentration profile of the δ layer determined with the electron probe microanalysis by Bastin et al. Arrow 1 indicates where the pallisade structure starts being visible while arrow 2 locates the beginning of the disrupture of the palisade structure.

Bastin et al has observed a difference in morphology between the regions of δ_p and δ_k. Figure 2.4b shows the
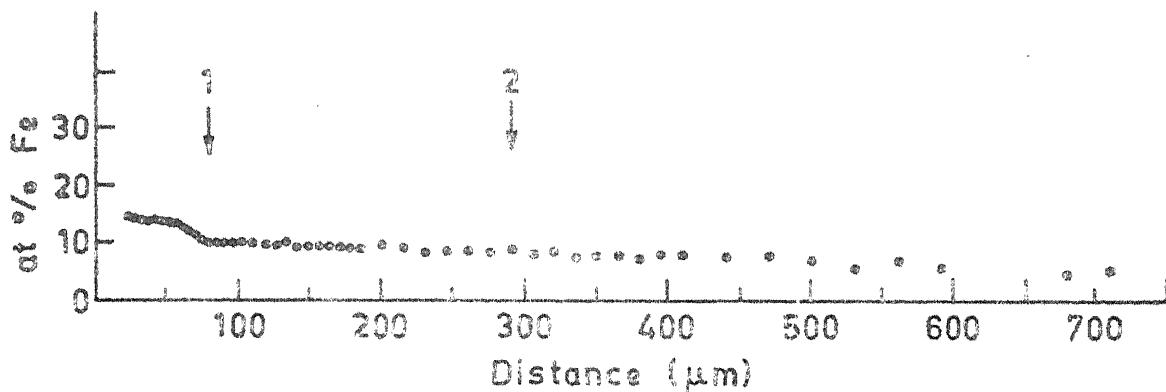
Fig. 2.4a. Concentration profile of the δ-layer
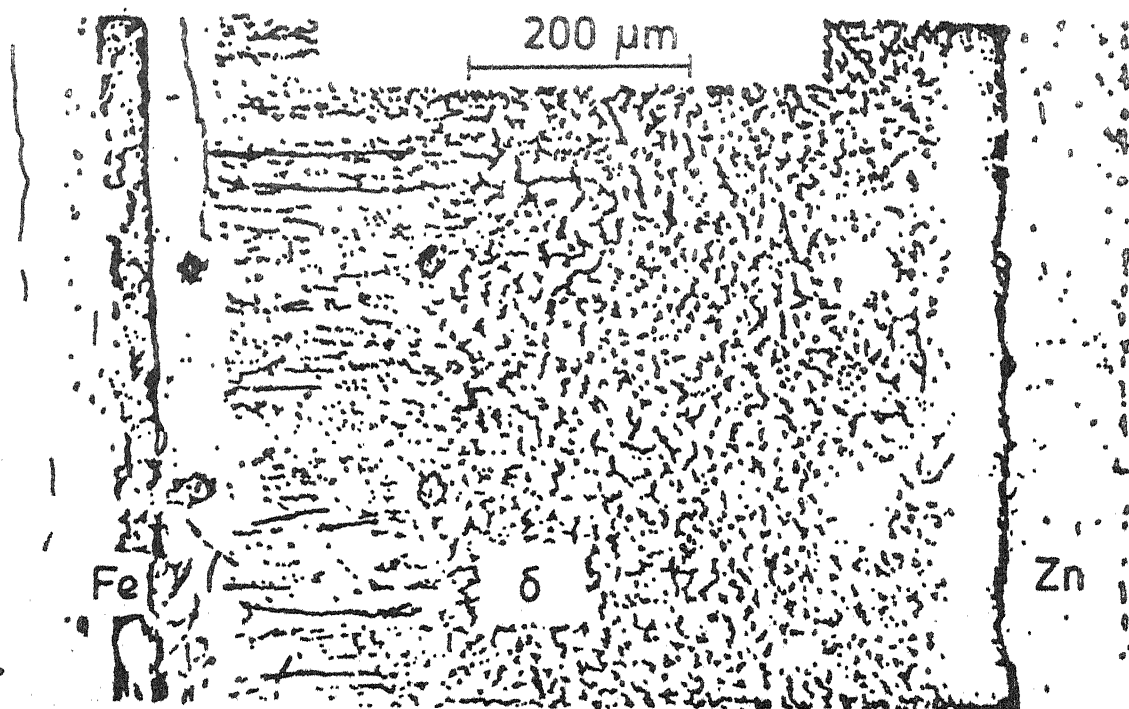
Fig. 2.4b. Morphology of the δ-phase.
        (Optical micrograph of a specimen hot dip
        galvanized during 4 h at 500 °C)[10].

sketch of an optical micrograph obtained by Bastin, which shows a preferred orientation steadily increasing from the Zn-rich side to the Fe-rich side of the layer. At the extreme Zn-rich side the palisade structure is completely broken up and Zn is present between the δ grains.

Gellings et al[11] pointed out that it was possible to synthesis a homogeneous compound of a composition which lies, according to Ghoniem, in the two phases $(\delta_{1p} + \delta_{1c})$ region. He has found the variation of microhardness values, both on the synthesized δ_1 phases and on a galvanized layer system. His values of microhardness in the δ region of Fe-Zn system is presented in Table 2.2 below.

Table 2.2.   Microhardness HV 0.01

Compound	Microhardness
"δ_{1c}" (11.34 wt %)	300
"δ_{1p}" (7.22 wt %)	284
Fe ⎫	67
"δ_{1c}" ⎬ galvanized samples	300
"δ_{1p}"	260
δ ⎭	200

Both Bastin's and Gelling's investigations supported to the view that the terms δ_{1k} (compact) δ_{1p} (palisade) are d
 distinguishing terms for the same phases in different physical states.

2.6.   Instability of the δ-phase:

The diffusion experiment[12] using 'Mo' wires as inert markers spot-welded to Armco iron before galvanizing has shown that the main diffusion process is that of the Zn moving through the galvanized layer towards the iron interface. Study of the increase in thickness of the intermetallic phase layers and the decrease in thickness of iron have shown[13] the relationship between the movement of interfaces. The Γ-phase is formed at the Fe/Γ interface and consumed at the Γ/δ_1 interface, while the ζ forms all the time at the ζ/Zn interface but converts to δ_1 at the δ_1/ζ interface.

The reason for the change of reaction rate from parabolic to linear and back to parabolic with increasing temperature has been the subject of much speculation and dispute. The explanation is given based on the importance of a continuous layer of the ζ-phase. When ζ-phase[1] is absent on porous, an unstable situation arises between the δ_1 and the molten η-phase, leading to an increased rate of attack. This increased attack causes the stresses in the growing layer, owing to volume changes to build up at a rate at which they can no longer be accommodated. The stresses, within the surface layer, ultimately causes rupture to occur, probably at the δ_{1k}/δ_{1p} interface, causing the δ_{1p} phase to buckle[14]. Cracks appear in the δ_{1p} and η-penetrates under it to the δ_{1k} and reacts to form a new δ_{1p} layer.

Eventually the buckled δ_{1p} breaks and η attacks directly at the δ_{1k}/δ_{1p} interface where the stresses prevail and cause the δ_1 to peel off and float into the melt. The detached layers of δ_{1p} still undergo attack by η and end with various forms of disintegration.

The reason for the reversal in the mechanism above 530°C is not completely clear but it has been suggested[1] that if the true transition temperature for δ is 530°C, then above this temperature the $\delta_1 - \eta$ boundary gives stable equilibrium conditions. It is also probable that at higher temperatures the δ_1 becomes more plastic and can accommodate the stresses without buckling.

2.7. X-ray Diffraction Work on the δ-phase of the Fe-Zn System by Different Investigators:

In 1938, Bablik et al[15], on the basis of single crystal work state that the δ phase has a hexagonal unit cell with dimensions a = 12.80 Å, c = 57.60 Å and the unit cell contains 550 atoms.

In 1976, Bastin et al[10] studied the δ phase with their self prepared single crystals. For preparation of single crystals, they first prepared an alloy containing 2 wt % Fe. The alloy constituents were heated in an evacuated and sealed silica capsule at 815°C during 92 hours. Then the completely homogenized melt was slowly (in 1½ hours time) cooled to 650°C, next very slowly to 550°C and subsequently quenched in water. The solidified lump was immersed in diluted HCl which caused the η phase (solid solution of

Fe in Zn) to dissolve much more rapidly than the δ phase. Through this process they extracted the δ crystals from the η matrix, and using a stereomicroscope some well-shaped crystals were selected for taking single crystal rotation and Weissenberg photographs.

It was found from the single crystal analysis, that most of the crystals clearly showed hexagonal symmetry. They found an average value of a = 12.815 Å and c = 57.35 Å for the primitive hexagonal unit cell. Further they showed that during hot dip galvanizing at temperatures between 460°C and 530°C, the δ layer is produced with a strong fibre texture in which the (h00) planes are oriented parallel to the original Fe/Zn interface. The strongest texture was observed at 500°C at the Γ_1/δ interface with a gradual decrease with increasing distance from this interface.

In 1977, the same investigators[4] studied the δ-phase of Fe-Zn system with suitable single crystals obtained like the previous manner. Single crystal rotation and Weissenberg photographs were taken with Fe-filtered Co radiation. The extraplotted values of 'a' and 'c' parameters obtained by them are given in Table 2.3 together with the equilibrium temperatures of the δ crystals and their compositions. Figure 2.5 gives a graphical representation of the results obtained. The error in 'a' and 'c' is estimated to be within ±0.00015 Å and ±0.00075 Å respectively, with a relative error of about 0.12% which is also indicated in the figure. From the

Table 2.3.   Single Crystal Data for δ Crystals Prepared at
              Various Temperatures.[4]

T in °C	Composition in at % Fe	a in 10^{-10} m	c in 10^{-10} m	c/a	Unit cell volume in 10^{-30} m³
515	8.20	12.8007	57.303	4.4766	8132
550	9.30	12.8098	57.161	4.4623	8123
570	9.60	12.7940	57.056	4.4596	8088
600	10.25	12.8086	57.013	4.4516	8098
625	11.38	12.8094	56.997	4.4496	8099
660	13.13	12.7738	56.957	4.4589	8049

observations, there is no indication found in support of the view that the δ phase field would be split up into two distinct phases δ_p and δ_k as has been suggested by Ghoniem and Lohberg[3]. The minimum of the c/a ratio obtained at about 11 at % Fe may be an indication of some ordering process within the δ crystal structure, which would lead to a minimum in structural defects.

Gellings et al[5] in 1979 have investigated δ_1 phases by X-ray powder diffraction using CuK_α radiation. The diffraction patterns were indexed using the data obtained by Bablik[15] and Bastin[10] and a close agreement was obtained between the data calculated from the structures of Bablik and Bastin and those experimentally determined by Bablik on δ_1 phases. The fact that the diffraction patterns of the δ_1 phase are identical over the whole concentration range proved the nonexistence of two δ_1 phases with different structures.

2.8.   X-ray Work on ζ, Γ and Γ_1 Phases of Fe-Zn System:

Gotzl et al[16] and Brown[17] have shown that the ζ-phase has a monoclinic unit cell with cell parameters a = 13.42; b = 7.608; c = 5.061 $\overset{o}{A}$ and β = 127.3°; space group C2/m. Brown has determined the complete structure of this compound.

In early 1978, Bastin et al[18] studied the ζ-phase of the Fe-Zn system with single crystal prepared in the same manner as that of the single crystals of δ (Chapter 2.8). Preliminary unit cell data from the Weissenberg and rotating
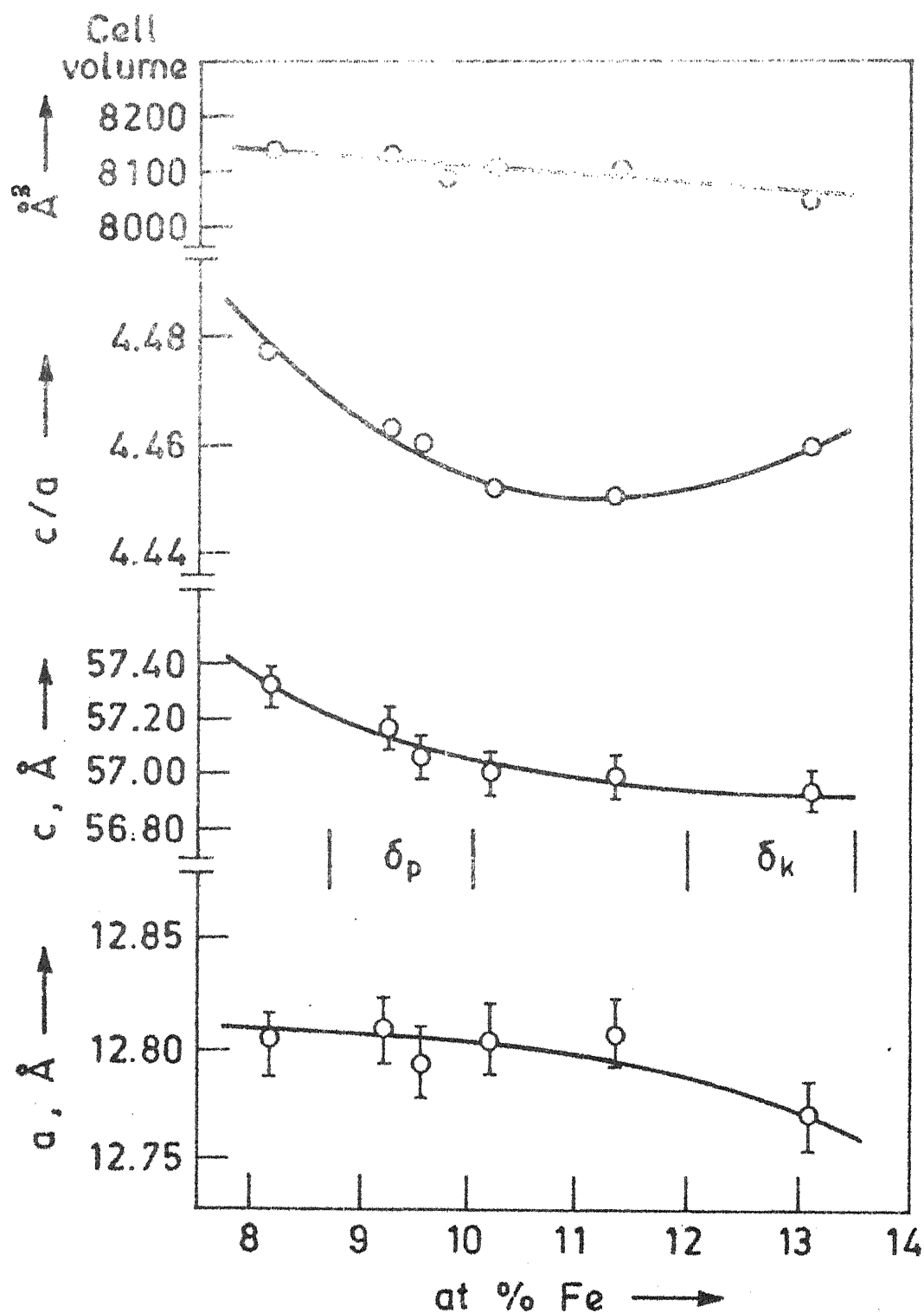
Fig. 2.5. Single crystal data for δ crystals of various compositions (for conversion into S.I. units: $1A = 10^{-10}m$).
By Bastin et al

crystal photographs were used index diffractometer recordings from powders of ζ phase and was resulted in the following data: a = 13.4051; b = 7.604; c = 5.069 Å and β = 127.22°. These geometric data showed good agreement with those of Brown Bastin carried out the hot dip galvanizing experiments on iron strips (purity 99.6 wt %). The strips were cleaned, pickled and immersed in a bath of molten Zn (purity 99.9 wt %) for times between 5 minutes upto 1 hour and at temperatures ranging from 430°C to 480°C. At the end of the experiment the strips were rapidly withdrawn from the bath, quenched in water and adhering Zn layer was then ground off and successive sections parallel to the original Fe/Zn interface were subjected to texture analysis.

Bastin used ordinary X-diffractometry, texture goniometry and photographical methods for this study and found that during hot dip galvanizing of iron between 430°C and 480°C, a ζ layer is produced with a texture which is rotationally symmetric around the direction of diffusion. The ζ crystallites were no longer found to have their c axis aligned parallel to the direction of diffusion but were found to have tilted and the tilting angle was observed to increase steadily with increasing distance from the δ/ζ interface. A similar increase of tilting angle was observed with increasing temperature

In 1979, Gellings et al[5] synthesized the ζ-phase of Fe-Zn system by liquid-hot-pressing method and investigated

the $\bar{\gamma}$-phase of 6.15 wt % Fe by means of X-ray powder diffraction using CuK$_\alpha$ radiations. The powder pattern has been calculated using Brown's data. The unit cell parameters and the X-ray diffraction pattern of Gellings are shown in Table 5.2 in Chapter 5 of this report. Gellings value of unit cell parameters generally agrees well with that of Brown.

In 1974, Bastin et al[19], by means of the diffusion couple techniques and X-ray diffraction studies, established the presence of Γ_1 phase containing 18.5 to 23.5 at % Fe at 380°C in the Fe-Zn system. The lattice of the Γ_1 phase found to be related to that of the Γ phase in that its cell parameter was obtained by doubling that of the b.c.c. unit cell of Γ phase, yielding a value of a = 17.963 Å. The Γ_1 phase is reported to have a unit cell of f.c.c. type. The homogeneity range of Γ_1 phase was found to decrease with increasing temperature whereas the reverse was observed for the Γ phase.

2.9.   Density Measurement by Different Investigators:

E.C. Ellwood[20] measured the densities of Al-Zn alloys by Archemidics weight loss method using distilled water. The results were corrected for the density of water at the temperature of the measurement and a correction was made for the thermal expansion of alloys between the temperature of measurement and 25°C. Thus the final density figures were those for 25°C. The results were compared with theoretical density calculated from the expression

$$\rho = mMN/a^3$$

where ρ = density

m = mass of atom of unit atomic weight (1.66033x10^{-24} gm)

M = a composite atomic weight for the atoms in the
alloy calculated from their international atomic
weights and atomic percentages

N = number of atoms per unit cell and

a = lattice constant in Å.

The density results were interpreted in terms of percentage
vacant lattice sites which are calculated from the expression

$$\% \text{ V.L.S.} = 100 (\rho_t - \rho)/\rho_t$$

where ρ_t and ρ are the theoretical and actual densities
respectively.

J.O. Betterton and William Hume-Rothery[21] has
determined the density of Cu-Ga samples using liquid ethylene
dibromide instead of distilled water. The adhering gas
bubbles were removed by prolonged evacuation. The probable
error of the method was estimated as being of the order of
1 part in 5,000 and the observed differences between duplicate
measurements lay between 1 part in 4,000 and 1 part in 80,000.

2.10. Scope of the Present Investigation:

From the work done by the previous investigators
on the δ-phase, especially from the investigations of Bastin
et al[4] in 1977 it is quite probable that there may be some

ordering process within δ phase, which can be accounted for the instability of the δ phase at the temperatures of interest of hot dip galvanizing. If any such ordering process is detected, the temperature composition and the nature of such a process is predicted, it will enable useful guidelines for further investigations on the intermetallic compounds of the Fe-Zn system for improving the galvanized coatings against corrosion. The present investigation aimed at finding out the possibility of any order-disorder phase transformation in the δ phase of the Fe-Zn system using X-ray diffraction and density measurement techniques.

CHAPTER   III

EXPERIMENTAL WORK

3.1.   Preparation of the Representative Fe-Zn Alloys:

To represent the various phases present in the zinc-rich part of the Fe-Zn binary system, alloys of respective compositions are synthesized[22] by the following manner.

Electrolytically pure iron of the following composition:

Carbon	=	0.003%
Phosphorus	=	0.005%
Sulphur	=	0.005%
Manganese	=	0.005%
Copper	=	0.005%
Silicon	=	0.005%

and 99.999% zinc were used for preparing the Fe-Zn alloys.

The pure iron lumps were crushed or filed into powder (the lumps being porous broke easily). Pure zinc cylinders of about 1 cm long and 5 mm diameter were made. Holes were drilled in it and weighed amount of pure iron powder were filled in these blind holes. Then the zinc cylinders containing iron powder were pushed into clean, quartz tubes. The quartz tubes were sealed under vacuum and the iron-zinc mixture was melted. After melting they were quenched in water. The details of the melting and

heat treatment of the alloys are presented in the tabular
form in Table 3.1.

The furnace used had a long constant-temperature
zone and the temperature was controlled to $\pm 2°C$.

Quenched ingots after melting, were broken into small
pieces and re-sealed in the quartz tube under vacuum. About
10 mm internal diameter and 1.25 mm thick quartz tubes were
used.

The sealed quartz tubes were put inside the holes,
drilled in cylinders of either aluminium or copper (depending
upon the annealing temperature). The ends of the metal
cylinders were closed with appropriate metal stoppers and the
cylinders containing the samples were put inside the furnace.
Both ends of the furnaces were closed with the refractory
blocks. The temperature was measured by putting a calibrated
thermocouple inside a hole drilled in the metal block. When
the annealing was complete, the quartz tubes were pulled out
with the help of wires attached to them and quenched in water.

For low-temperature annealing, salt baths were used.
For all cases the temperature were constant to $\pm 1°C$ for weeks.

3.2. Analysis:

The samples were examined[23] under optical micro-
scope and Scanning Electronmicroscope. No indication of
segregation was found. Since the metals were melted under
vacuum in sealed silica tubes, there was very little loss

Table 3.1.   Melting and Heat Treatment History of Fe-Zn Alloys.

Specimen Identification Number	Composition of alloys (in at % Fe)	Melting	Heat Treatment
6.1	7.07	At 880°C for 2 days, at 900°C for 3 days and at 920°C for 5 days water quenched.	Annealed at 447°C for 6 days and at 472°C for 21 days. Water quenched.
6.6-o-350	7.68	At 920°C for 10 days water quenched.	1. Annealed at 475°C for 24 days and cooled to 250°C in 8 days. 2. Again annealed at 350°C for 27 days and water quenched.
6.6-w-475	7.68	Same as above.	Annealed at 475°C for 15 days and water quenched. Again annealed at 473°C for 14 days and water quenched.
8-o-475 (8-o-4)	9.24	At 925°C for 8 days and water quenched.	Annealed at 525°C for 15 days. Then furnace cooled in 7 days. Again annealed at 473°C for 14 days and water quenched.
8-w-475-350 (8-w-43)	9.24	Same as above.	Annealed at 527°C for 14 days, water quenched. Further annealed at 473°C for 14 days water quenched and again annealed at 350°C for 22 days followed by water quenching.

Table 3.1 (continued)

Specimen Identification Number	Composition of alloys (in at % Fe)	Melting	Heat Treatment
9-w-550 (9-w-5)	10.29	At 930°C for 10 days, water quenched.	Annealed at 566°C for 5 days. Air cooled. Again annealed at 555°C for 10 days, water quenched. Then annealed at 552°C for 6 days and furnace cooled. Again annealed at 552°C for 14 days, water quenched.
9-w-53	10.29	Same as above.	Same as above followed by further annealing at 350°C for 19 days and water quenched.
9-o-550 (9-o-5)	10.29	Same as above.	Annealed at 555°C for 7 days and slowly cooled at 280°C in 4 days. Again annealed at 551.3°C for 21 days.
9.5-550 (I)	10.94	At 943°C for 10 days. Water quenched.	Annealed at 567°C for 21 days. Then the alloy was allowed to cool in the furnace.
9.5-550(II)	10.94	Same as above.	Same as above.
9.5-550-350 (9.5-53)	10.94	At 943°C for 10 days. Water quenched.	Annealed at 567°C for 21 days, furnace cooled and further annealed at 350°C for 21 days and water quenched.

Table 3.1 (continued)

Specimen Identification Number	Composition of alloys (in at % Fe)	Melting	Heat Treatment
10-o-550 (10-o-5)	11.63	At 900°C for 3 days further melted at 950°C for 7 days. Water quenched.	Annealed at 590°C for 15 days, furnace cooled to 250°C in 8½ days and then annealed at 551.3°C for 21 days.
10-w-550 (10-w-5)	11.63	Same as above.	Annealed at 590°C for 7 days, water quenched. Annealed at 552°C for 20 days and water quenched.
11-w-550 (11-w-5)	12.67	At 960°C for 11 days. Water quenched. Again melted at 950°C for 4 days, water quenched.	Annealed at 610°C for 21 days, water quenched. Again annealed at 555°C for 16 days and water quenched.
11-w-550-350 (11-w-53)	12.67	Same as above.	Annealed at 610°C for 21 days, water quenched. Then annealed at 555°C for 16 days, water quenched. Again annealed at 350°C for 23 days and water quenched.
11-o-550 (11-o-5)	12.67	At 960°C for 11 days, water quenched. Again melted at 950°C for 4 days, water quenched.	Annealed at 610°C for 17 days, furnace cooled in 7 days to 480°C. Again annealed at 551°C for 18 days, water quenched.

Contd...

Table 3.1 (continued)

Specimen Identification Number	Composition of alloys (in at % Fe)	Melting	Heat Treatment
14-w-605 (14-w-6)	16.01	Melted in-between 900-1030°C for 10 days, water quenched.	Annealed 595°C for 8 days and at 615°C for 12 days, water quenched. Again annealed at 605°C for 10 days and water quenched.
14-w-475 (14-w-4)	16.01	Same as above.	Annealed at 600°C for 20 days, water quenched. Further annealed at 447°C for 6 days and at 474°C for 12½ days, water quenched.
14-o-550 (14-o-5)	16.01	Same as above.	Annealed at 610°C for 17 days and cooled to 480°C in 7 days then air cooled. Again annealed at 550°C for 16 days, water cooled.
14-o-350 (14-o-3)	16.01	Same as above.	Annealed at 610°C for 17 days and cooled to 480°C in 7 days and air cooled. Again annealed at 353°C for 25 days and water quenched.

of material. Therefore the composition is taken to be same
as that calculated from the weights of iron and zinc used
for melting.

The Atomic Absorption Spectrophotometer and the
Proton Induced X-ray Emission analyser (PIXE) were used to
further confirm the composition of some of the alloys.

3.2.1. Atomic Absorption Spectrophotometer (AAS):

The atomic absorption spectrophotometer, Model IL
751AA/AE manufactured by Instrumentation Laboratory Inc.,
installed in The Advanced Centre for Materials Science, I.I.T.
Kanpur was used for the experiment.

3.2.1.1. Principles of Atomic Absorption[23]: Atomic
absorption spectrophotometry makes use of the fact that
neutral or ground state atoms of an element can absorb
electromagnetic radiation over a series of very narrow,
sharply defined wave-lengths. The sample, in solution, is
aspirated as a fine mist into a flame where it is converted
to an atomic vapour. Most of the atoms remain in the ground
state and are therefore capable of absorbing a radiation of
a suitable wave-length. This discrete radiation is usually
supplied by a hollow cathode lamp, which is a sharp line
source consisting of a cathode containing the element to
be determined along with an anode (usually tungsten).

When a sufficient voltage is impressed across the
electrodes, the filler gas is ionized and the ions are

accelerated towards the cathode. As these ions bombard the cathode, they cause the cathode material to "sputter" and form an atomic vapour in which atoms exist in an excited electronic state. In returning to the ground state, the lines characteristic of the elements are emitted and pass through the flame where they may be absorbed by the atomic vapour. Since, generally, only the test element can absorb this radiation, the method become very specific in addition to being sensitive.

3.2.1.2. Apparatus: The schematic[24] of the basic apparatus is shown in figure below:

| Light Source | → | Atom Cell | → | Monochromating Device | → | Detector and Readout Device |
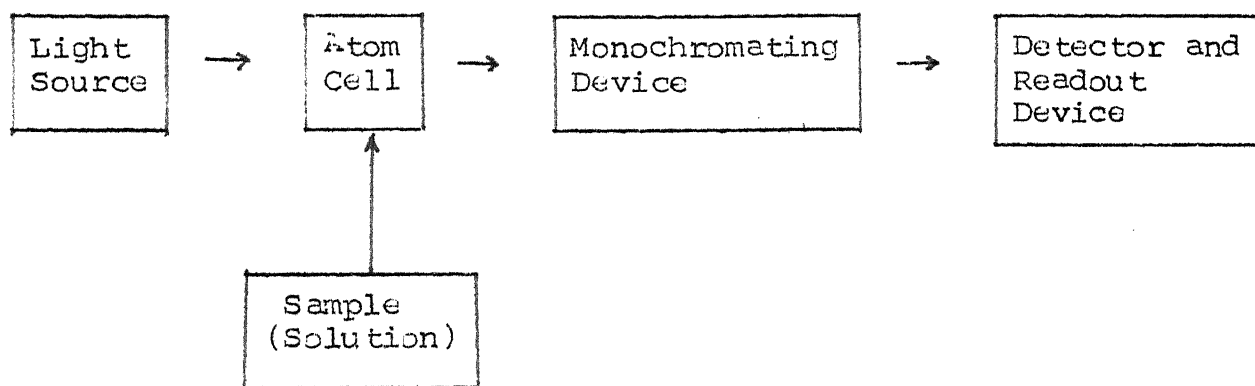
Sample (Solution)

Figure: Schematic diagram of AAS.

The sample to be tested is in the form of solution which is fed into the atom cell and atomized. If the atoms contained in the atom cell are to absorb radiation, they must be irradiated with the light of the same wave-length that has been atomized. This radiation is obtained from

a 'light source' which may emit the spectrum of single
element.

The light transmitted after the atomic absorption
process has occurred, will often be composed of radiation of
both the required wavelength (i.e. the absorption line(s))
and a number of unwanted wavelengths due to stray daylight
or due to other spectral lines (emitted by the light source
or atom cell).

It is necessary, therefore, to select the wavelength
of the radiation from the atom cell before measuring the absorption
signal. This is done with a 'monochromating device', which
is placed in the direct optical path from the source to the
cell for absorption measurements. The device used to convert
the radiation constituting the absorption signal into a form
that can be easily measured (and recorded if necessary) is
known as the 'detector'. The detector device consists of
photoelectric devices that convert the optical signal to an
electrical signal which is analysed by the associated
electronic assemblies.

3.2.1.3. Experiment: Tables 3.2 and 3.3 shows the
standard conditions used for operation.[25] Standard solutions
were prepared from 99.9% pure iron specimen. 1 gram of pure
iron was dissolved in about 50 ml of 1:1 HCl and diluted to
exactly 1 litre with double distilled water. This solution
contained 1000 ppm of iron. The absorption coefficient Vs.
concentration profile for element iron is linear upto a

Table 3.2.   Standard Atomic Absorption Conditions for Fe
Determination by Flame Atomization.

"Instrumental Parameters"

Light source   : Hollow cathode

Lamp current   : 10 mA

Wavelength   : 248.3 nm

Slit width   : 30 μm

Burner head   : Single slot

IL lamp number   : 62810

Band pass   : 0.3 nm

IL number   : 43005-02

Flame description   : Air-acetylene
                              Oxidizing, Fuel lean, Blue

Photomultiplier Voltage (HV) : Once the lamp current, wave-
                                length, and slit width have
                                been set, adjust the appropriate
                                HV control until the log inten-
                                sity meter reads between 0.2
                                and 0.8 volt.

Sensitivity   : The sensitivity (at 0.0044
                              Absorbance = 1% absorption) is
                              about 0.04 μg/ml for the instru-
                              mental parameters described
                              above.

                              A standard containing 1 μg/ml
                              of Fe will give a reading of
                              approximately 0.1 A.

Linear range   : The working range for Fe is
                              linear upto a concentration of
                              approximately 5 μg/ml (when
                              using an aqueous solution and
                              the instrumental parameters
                              described above).

Table 3.3.   Standard Atomic Absorption Conditions for Zn
Determination by Flame Atomization.

"Instrumental Parameters"

Light source   :   Hollow cathode

Lamp current   :   3 mA

Wavelength   :   213.9 nm

Slit width   :   320 μm

Burner head   :   Single slot

IL lamp number   :   62811

Band pass   :   1 nm

IL number   :   43005-02

Flame description   :   Air-acetylene
                                          Oxidizing, Fuel lean, Blue

Photomultiplier Voltage (HV) :   Once the lamp current, wave-
                                          length, and slit width have
                                          been set, adjust the HV control
                                          until the log intensity meter
                                          reads between 0.2 and 0.8 volt.

Sensitivity   :   The sensitivity (at 0.0044
                                          Absorbance = 1% absorption) is
                                          about 0.008 μg/ml for the
                                          instrumental parameters
                                          described above. A standard
                                          containing 0.25 μg/ml of Zn
                                          will give a reading of approxi-
                                          mately 0.1 A.

Linear range   :   The working range for Zn is
                                          linear upto a concentration of
                                          approximately 1 μg/ml (when
                                          using an aqueous solution and
                                          the instrumental parameters
                                          described above).

maximum of 5 ppm of iron in the solution. Four standard solutions were prepared containing 1 ppm, 2 ppm, 3 ppm and 4 ppm of iron and fed to the AAS and the absorption coefficient Vs. concentration profile of iron was obtained.

The solutions of the alloys whose composition to be measured were prepared similar procedure, on the basis of known composition (Table 3.1).

Example: Preparation of AAS solutions of Fe-Zn alloy containing 10.94 at % Fe (9.5 wt % Fe).

About 0.5 grams of the alloy containing 10.94% Fe was dissolved in 25 ml of 1:1 HCl and the solution was made to 1 litre by double distilled water. The resulting solution contains about 95 ppm of iron -- Solution (A).

10 ml of solution (A) was mixed with 180 ml of double distilled water and the solution (B) containing 5 ppm of iron was obtained:

$$\frac{10 \times 95}{(180 + 10)} = 5 \text{ ppm} \text{ -- (B)}$$

160 ml of solution (B) was mixed with 40 ml of double distilled water and the solution (C) containing 4 ppm of iron was obtained:

$$\frac{160}{(40 + 160)} \times 5 = 4 \text{ ppm} \text{ -- (C)}$$

Similarly solutions containing 3 ppm, 2 ppm and 1 ppm were prepared.

These solutions were fed into AAS and their corres-
ponding absorption coefficients were obtained. From the
standard absorption coefficient Vs. concentration curve of
pure iron, the exact concentration of iron present in a
particular alloy was obtained.

3.2.1.4.   Results:

	Pure Iron
Solution standard	Absorption coefficient
2 ppm	0.032
3 ppm	0.068
4 ppm	0.094
5 ppm	0.118

Thus the standard concentration Vs. absorption
coefficient curve for iron was obtained. Using this curve,
the concentration of the Fe-Zn alloy containing 12.67 at % Fe
(11.0297 wt % Fe) obtained by the AAS was shown below:

Solution concentration based on Table 3.1	Concentration obtained by AAS	Concentration in wt % Fe	Concentration in at % Fe
5 ppm	5.103 ppm	11.2569	12.929
4 ppm	3.973 ppm	10.9552	12.589
3 ppm	2.957 ppm	10.8716	12.495

Average iron concentration of 11-W-5 alloy (12.67 at % Fe
by Table 3.1) was 12.671 at % Fe. Unfortunately due to

some fault in the AAS, inconsistent results were obtained
with other alloys. The experiment was carried out using pure
zinc as the standard element to be tested but similar irre-
producible results were given by the equipment. Since this
fault could not be detected, further analysis was abondened.

3.2.2.   Proton Induced X-ray Emission Analyser (PIXE):

It was intended to ensure the exact composition of
the Fe-Zn alloys and also detect the presence of impurities
if any, by the proton induced X-ray emission analyser in the
Nuclear Physics Laboratory, I.I.T. Kanpur.

The Model AN-2000 Van de Graff Accelerator manufac-
tured by High Voltage Engineering Corporation, U.S.A. was
used to produce high intensity source of positive ions.

Hydrogen gas is introduced into the ion source of
the Van de Graff accelerator. Radio-frequency power from
the r.f. oscillar supplies the energy to ionize the gas in
the ion source. A positive potential is applied to the probe
of the source, the positive ions are focussed and accelerated
by means of the electric field along the evacuated glass-
and-metal acceleration tube. Each metal electrode of the
tube is connected to a corresponding equipotential plane
whose d.c. potential is maintained by the voltage divider.
The positive ion beam is accelerated to extremely high
velocity by the potential difference 'V' between the terminal
and ground ends of the acceleration tube. The positive ions

leave the acceleration tube with a kinetic energy eV. Because the potential is d.c. in nature, the particles in the beam are homogeneous in energy at any instant.

For precise measurement and control of the ion beam energy, the beam is deflected by a magnetic field whose strength is held constant by an electronically regulated d.c. power supply. An insulated slit system at the exit part of the magnet permits ions of a particular mass-energy product to proceed to the specially designed scattering chamber.

The scattering chamber made of aluminium is cylindrical of diameter 20 cm, and with arrangements to couple a Si (Li) detector in standard liquid-nitrogen-cooled crysostat. The chamber has viewing ports, multiple target holder, graphite collimeter for Si (Li) detector and an externally operated filter wheel in front of the graphite collimeter.

Preparation of suitable targets is of prime importance in PIXE analysis. There exists no unique prescription for this purpose.

Laboratory Formvar films were used as the backing for the sample powders for preparing targets. Few drops of formvar solution (polyvinyl acetate dissolved to nearest saturation in methyl benzoate, toluene and ethyl alcohol in the ratio 5:12:8) were allowed to spread on the surface of deionized-double distilled water forming a thin layer (~ 25 $\mu g/cm^2$). The film was picked up on a target frame and allowed to dry. The film so produced was mechanically strong enough to withstand the alloy powders under investigation.

The alloy powders were first dissolved/mixed in deionized-distilled water and a small drop (5μlitre) of the solution was allowed to dry on the formvar backing. The sample was then sandwitched with another formvar film.

The proton beam impinges on the target placed at $45°$ to the incident direction. Before exposing the sample to the proton beam, the detector and the energy-channel number·calibration was carried out using ^{241}Am standard source.

The samples were fixed on the holder in the scattering chamber. The protons interacted with the atomic electrons of the target material either jecting or exciting them. This interaction produced X-radiations characteristics of the elemental composition of the target. The X-rays emerging out of the sample were detected by the lithium drifted silicon detectors and were analysed by the multichannel analyser (MCA) attached with the detector. The X-ray signals were printed by the teleprinter. The data were plotted in a graph paper manually.

There are four distinguishable peaks obtained corresponding to K_α and K_β characteristic X-radiations in each of the alloy. The absence of any other peaks (even traces) in the intensity Vs. Energy channels indicates that there are no impurities present in the Fe-Zn alloys.

The amount of the elements present in the alloy is indicated by number of X-ray counts. The larger the quantity of the material present, higher the number of counts. The

ratio of the areas occupied by the peaks represents the ratio of the amount of the elements present (in weight percents).

The alloy 11-w-5 of 12.67 at % Fe (or 11.0297 wt % Fe according to Table 3.1) was repeated three times and in each time completely different values of the amounts of iron and zinc were obtained (Figure 3.1). Other alloys also showed the same trend. The reason for such behaviour could not be found. However, none of the alloys gave peaks due to any other element.

3.3. X-ray Diffraction Work:

X-ray diffraction work was carried out on the alloy powders for finding out the crystal structure data of each intermetallic compound of the Zn-rich part of the Fe-Zn system and for accurate determination of their lattice parameters. It was intended to determine accurately the variation of the unit cell parameters of the alloys with composition and heat treatment.

3.3.1. Preparation of Powder Samples for X-ray Diffraction Work:

The lumps of the Fe-Zn alloys were crushed in a clean metal crusher and the powder was classified by the 325 size mesh sieve. There were no strains present in the powders since the alloys are brittle in nature and they were easily crushed.
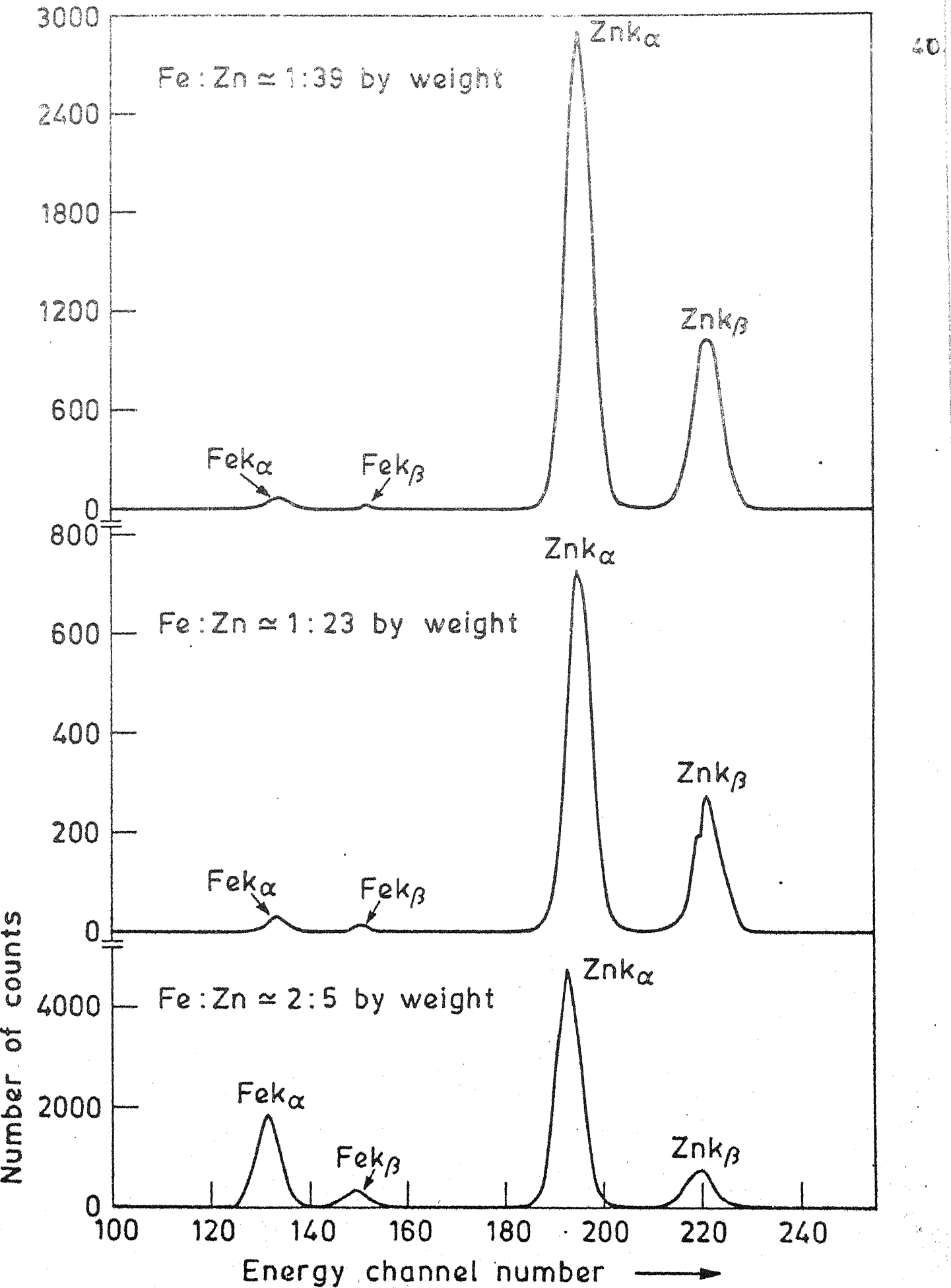
Fig. 3.1. PIXE analysis of 11-W-5 alloy repeated three times
containing 11.0297 wt % Fe/12.67 at % Fe (Table 3.1)

A perspex sheet of dimensions 50 x 25 x 5 mm was
chosen for the sample holder and a circular depression of
20 mm diameter and 2 mm thickness was made (the optimum
dimensions of a diffractometer sample holder according to
H.P. Clug and L.E. Alexander[28]). A small quantity of binder
(Krylon, Spray Coating No. 1302) was sprayed on the walls of
the circular cavity for good binding of alloy powder with the
sample holder. An excessive amount of powder was filled in
the cavity and tamped gently and thoroughly with the edge of
a spatula. Then some more powder was added to the cavity and
pressed gently with a clear glass slide. Again a small
quantity of binder was sprayed on the powder surface to keep
the powder surface intact. Then the surface was pressured
to be flat and the surplus powder was sliced off with a razor
blade. The sample was then ready for exposure.

3.3.2. Suitable X-ray Diffraction Conditions:

3.3.2.1. Selection of Target Material: The separation
between the neighbouring peaks and position of the peaks in
a diffraction pattern depend upon the wavelength of the
radiation used. Longer the wavelength of the target material,
greater is the separation between the lines. Out of the
two target materials iron and cromium which would give
maximum separation of the peaks at a particular 2θ value
cromium target was unfortunately not available in the X-ray
Lab. Moreover cromium shifts peaks to a higher angle by

only about 10^2 for a 2θ of $50°$ compared with iron but it
reduced the intensity. Therefore no special efforts were
made to use cromium target and all the work was carried out
by iron target.

By using proper filter material (MnO foil for Fe
target), almost 98% of the K_β radiations are filtered
and the intensity of K_{α_2} radiation was considerably reduced.[28]
The difference in 2θ due to difference in K_{α_1} and K_{α_2} of Fe
radiation at $2\theta \simeq 50'$ is only about $0.11°$. This is negli-
gible comparing with the difference in 2θ of the consecutive
peaks of any Fe-Zn alloy. So for calculation of 'd' values
of prominent, well resolved peaks, only K_{α_1} was taken into
account when the target was used with filter.

3.3.2.2. Range of 2θ Used for Scanning: A diffraction
pattern of the sample (8-o-4) was taken over the entire range
of 2θ (from $2\theta = 10°$ to $2\theta = 146°$) using 'Cu' target so as to
get maximum intensity and obtain maximum number of lines.
It showed that upto $2\theta = 40°$ there are very low intensity
peaks which are clustered together, between $40°$ to $56°$ there
are clear, several strong peaks and from $56° - 64°$ there
are weak peaks present. Above $64°$, the peaks are hardly
detectable from the background. Very weak and broad peaks
are present at $120°$. It is impossible to determine the 2θ
values accurately for these peaks.

The sample was again scanned over the entire range
using conditions so as to give maximum detectability of peaks.

However only very few weak peaks could be obtained at angles about 97° and 120°.

It was therefore decided to determine positions of the prominent peaks found between $2\theta = 44° - 64°$. In order to accurately determine the positions of these peaks, suitable diffractometer conditions were first determined.

3.3.2.3. Diffractometer Conditions: According to L.E. Alexander and H.P. Clug,[28] the best conditions are given in Table 3.4.

Table 3.4. Diffractometer conditions for best resolution with reasonably good intensity, according to L.E. Alexander and H.P. Clug[28]

Radiation used   : CuK_α

Source viewed laterally

Beam Slit   :   1° for $2\theta = 90°$ and 4° above 90°

Sollor slit   :   Meadium resolution (2.2° aperture)

Detector slit   :   0.025° below $2\theta = 90°$ and 0.05° above 90°

Automatic strip-chart recorder = 1/8 or 1/4° per minute

Scanning speed = 0.25° 2θ per minute.

However these conditions did not give satisfactory results with the 'XRD-5 General Electric' diffractometer. In order to determine the optimum conditions, diffraction pattern of a particular sample (8-o-4) within the range 44°-64° was taken with MnO filtered Fe-radiations using various combinations of Beam Slit width, Detector Slit width, Sollor Slit width, Scanning speeds, Charts speeds, Time constants and Count rates. The results are summarized in Table 3.5.

Table 3.5.   Diffractometer Conditions (XRD-5).

Target Material used: Fe   Target tube : Cu-7

Filter : MnO   Voltage : 40 kv

Range of 2θ : 44° - 64°   Current : 7 ma

Sl. No.	Beam slit width	Detector slit width	Sollar slit used	Scanning speed (degrees per minute)	Chart speed (inches per hour)	Time constant (seconds)	Count rate (counts per second)	Characteristics of the diffraction pattern
	3° 1°	0.2° 0.1° 0.05° 0.02°	MR HR	4.0 2.0 0.4 0.2	180 120 60 30 24 12 6	8 4 2 1 0.5	2000 1000 500 200 100	Available choices with XRD-5 diffractometer
(1)	3°	0.05°	MR	0.2	12	4	100	Best resolution possible with reasonably good intensity
(2)	3°	0.1°	MR	0.4	30	4	100	Poor resolution
(3)	3°	0.1°	MR	2.0	30	2	100	Peaks are too much compressed
(4)	3°	0.1°	MR	4	120	2	100	Low intensity and poor resolution
(5)	3°	0.2°	MR	0.4	60	2	100	Very broad peaks and low intensity

Table 3.5 (continued)

Sl. No.	Beam slit width	Detector slit width	Sollar slit used	Scanning speed (degrees per minute)	Chart speed (inches per hour)	Time constant (seconds)	Count rate (counts per second)	Characteristics of the diffraction pattern
(6)	3°	0.2°	MR	0.4	30	2	100	Resolution is not as good as (1)
(7)	3°	0.2°	MR	2.0	120	2	100	Peaks are too wide and resolution is poor
(8)	3°	0.2°	MR	2.0	60	2	100	Resolution is not as good as (1)
(9)	1°	0.02°	HR	0.4	30	2	100	Hardly any peak visible
(10)	1°	0.1°	HR	0.4	30	4	100	Hardly any peak visible
(11)	1°	0.1°	MR	0.4	30	2	100	Low intensity and poor resolution
(12)	3°	0.05°	MR	0.2	12	4	200	Resolution is not as good as (1)
(13)	3°	0.05°	MR	0.2	12	8	100	-do-
(14)	3°	0.05°	MR	0.2	12	2	100	-do-
(15)	3°	0.05°	MR	0.2	30	2	100	-do-
(16)	3°	0.05°	MR	0.4	12	4	100	-do-
(17)	3°	0.05°	HR	0.2	12	4	100	Low intensity
(18)	1°	0.02°	MR	0.2	12	4	100	-do-

Table 3.5 (continued)

By examining the table the following conclusions can be drawn:

Count Rate : The optimum count rate is 100 cps which gives maximum intensity. By using this one can approach maximum resolution conditions without loosing too much intensity.

Sollor Slit : High resolution sollor slit (HR) reduces intensity to a negligible value. With medium resolution sollor slits, high resolution can be obtained by suitable combinations of Beam slit and Detector slit.

Chart Speed : Most suitable chart speed with other parameters which increase resolution is 12"/hour.

Scanning Speed : Higher scanning speeds tend to reduce the solution very much. High scanning speeds also reduces intensity with any particular combination of other parameters. Therefore the most suitable scanning speed is 0.2°/minute.

Beam Slit : Wider beam slit increases the intensity without sacrificing much of resolution. 1° wide beam slit limits intensity very much so 3° beam slit is found to be suitable.

Detector Slit : Intensity increases with the width of the detector slit but the resolution becomes poor. The optimum width of the detector slit for good resolution without sacrificing the intensity is 0.05°.

A critical examination of the Table 3.5 shows that the following diffractometer conditions gives the best resolution with reasonable intensity with the XRD-5 diffractometer.

Target material	:	Fe
Filter	:	MnO
Cathode tube	:	CA-7
Voltage	:	40 kV
Current	:	7 mA
Beam slit	:	3°
Detector slit	:	0.05°
Sollor slit	:	Medium resolution S.S.
Scanning speed	:	0.2° per minute
Chart speed	:	12" per hour
Time constant	:	4 seconds
Count rate	:	100 counts per second

Further work was carried out using only these conditions.

Calibration of Diffractometer:

It is essential to calibrate the diffractometer for accurate 2θ measurements. The diffractometer was thoroughly aligned for zero adjustments. The Goniometer was set for the following conditions:

Beam slit	=	1°
Sollor slit	=	High Resolution S.S.
Detector slit	=	0.02°
Target	=	Fe
Filter	=	a copper foil

A direct beam of X-ray was sent to the detector through the slit system and a maximum number of counts were registered in the $2\theta = 0°$ position by suitably adjusting the base screws of the goniometer.

It was found that the flow of paper chart is not synchronized with the goniometer movements and the flow chart lags behind the goniometer at increasing 2θ values. Further this lagging of flow chart was found nonlinear. So the exact value of 2θ by which the flow chart lags behind the goniometer was noted for each degree of 2θ and this correction was applied to 2θ for the determination of exact 2θ value.

To measure accurately any systematic shift in the 2θ positions of the goniometer, it is essential to calibrate the goniometer with a standard sample whose accurate peak positions are known for a given target material. The single crystal of parmquartz (a mineral of quartz, SiO_2) was used for this purpose (since it shows strong peaks in almost all the ranges of 2θ) and the systematic corrections for 2θ shifts in the goniometer were determined.

A typical tracing for samples 8-o-4 and 8-w-43 are shown in Figures 3.2 and 3.3 respectively. The diffracto- meter tracing of alloy 6.1 W is shown in Figure 3.4.

The X-ray diffraction room is all the time air- conditioned and the temperature all the time remained $26°C \pm 2°C$.

3.4. Density Measurements:

3.4.1. Suitable Conditions for the Density Measurement of Powders:

Density of solid substances can be measured by simple Archemedic's weight-loss method. But in the case of powder samples and porous materials, the density measured by this technique would be less than true density of the material because of the following reasons:

(1) Presence of holes and crevices in the material

(2) Presence of air bubbles between the individual particles if their size is finer.

As we make the powder size finer and finer, the chances of the particle containing small holes, cavities and crevices becomes less but the chances of air bubbles trapped in-between particles becomes immersed in a liquid becomes more. So an optimum particle size is required for good results.

The alloys were crushed and made fine enough to exclude any holes inside and its surface was examined under a binoculars to make sure that it has no holes or crevices.

The density measurement of the alloys were carried out, first by using double distilled deionized water. Deionized water was used since its reaction with the alloy sample would be minimum. It was found that the ~~water~~ air bubbles in-between the particles were not completely removed by immersing the powders in water in atmospheric pressure.

Then it was decided to immerse the powders under vacuum so
that all the air bubbles between the particles would be
removed. But at sufficiently high vacuum, water started
evaporating and disturbed the vacuum pump.

So it is essential to select a suitable liquid for
density measurements which

1) should not react with the Fe-Zn samples,

2) should have low vapour pressure so that it would not
   evaporate at moderate vacuum ($10^{-3} - 10^{-4}$ torr),

3) should wet the powders easily and

4) should be denser than water for accurate results.

From the literatures of previous investigators,[21] it
is found that ethylene dibromide liquid is preferred for the
accurate density measurements, satisfying conditions 1) to 4),
unfortunately this liquid ordered about three months before,
has not reached by/the till time the author started writing this
report.

It was found that the rotary vacuum pump oil satis-
fies all the requirements except/4) condition (i.e. its density is less
than that of water). So the density measurements of all the
alloys were carried out using this oil. The apparatus
specially designed for immersing the powder samples under
vacuum is shown in Figure 3.5.

3.4.2. Procedure Used:

A flat bottomed, light glass tube of 30 mm length
and 10 mm internal diameter was hanged by a light copper

wire in a single span electrical balance (Model: AINSWORTH, Type 24 N Analytical balance) and its weight in air was measured (w_5). Then the glass-tube was weighed in the liquid by partially immersing the wire (w_2). The glass tube was cleaned thoroughly with acetone, dried and weighed in air (w_1).

The alloy samples of suitable particle size were transferred into the tube and weighed in air (w_3). Then the glass tube with samples are kept in the apparatus designed for immersing the powder sample into the liquid in vacuum. The liquid was taken in the side tube (Figure 3.5). At first the powder samples and the liquid were evacuated separately and the liquid was slowly poured into the weighing glass-tube containing the powder sample just to immerse the samples by rotating the side tube. Vacuum was maintained in the tube for sufficiently longer time (about one hour) for all the air bubbles to raise to the surface. Then the remaining liquid in the side tube was also transferred into the glass-tube.

The glass-tube with the samples then immersed in a beaker containing the same liquid and the weight of the glass tube and samples in liquid was found (w_4). The liquid in the beaker used for immersion was also previously, thoroughly degassed. All the time, the depth of the wire inside the liquid was maintained the same. The temperature and pressure under which the experiment carried out was noted all the time.

For obtaining accurate and reproducible values of density, the following precautions were taken:

(1) There was no air bubbles sticking the glass-tube, samples or the beaker.

(2) The wire used was thin, light and non-reactive with the liquid.

(3) The same length of the wire was immersed into the liquid all the time while making the weight measurements in liquid.

(4) The powder sample and the liquid were evacuated for sufficiently longer time to remove all the air inside the particles.

CHAPTER   IV

RESULTS

4.1.   Indexing of δ-phase of Fe-Zn System:

According to Bragg law,

$$\lambda = 2d \sin\theta \qquad (4.1)$$

where λ = wavelength of the radiation used for diffraction

d   = interplanar spacing of the powder sample

θ = angle of incidence.

$$\lambda = Fe\ K_{\alpha_1} = 1.93597\ \overset{\circ}{A}$$

$$\therefore\ d = (\frac{1.93597}{2}) \cdot \frac{1}{\sin\theta}\ \overset{\circ}{A} \qquad (4.2)$$

Bablik et al[15] (1938) have determined the crystal structure
of δ-phase of Fe-Zn system to be hexagonal with unit dimen-
sions a = 12.80 $\overset{\circ}{A}$; c = 57.6 $\overset{\circ}{A}$; 550 atoms per unit cell.

Bastin et al[10] (1976) have also determined the
crystal structure of the δ-phase to be hexagonal giving a =
12.815 $\overset{\circ}{A}$ and c = 57.35 $\overset{\circ}{A}$. Both these investigators have
noted that only hkl reflections with l = odd were systema-
tically absent.

For hexagonal structures,

$$\frac{1}{d^2} = \frac{4}{3}(\frac{h^2 + hk + k^2}{a^2}) + \frac{l^2}{c^2} \qquad (4.3)$$

Using the extinct conditions for diffraction,

$$h + 2k = 3n$$
$$\text{and} \quad l = \text{odd}$$

(4.4

(where n is an integer)

and with Bastin's values of 'a' and 'c' different values of 'd' for all the allowed combinations of h, k and l in the 2θ range 40° to 65° and the h, k and l range of 0 to 5, 0 to 5 and 0 to 35 respectively were obtained by the computer program (Appendix 1). Experimentally determined values of 'd' (using eqn. 4.2) were compared with the calculated values and the possible tentative indices (h k l) of the peaks were noted.

It was found that each peak could be associated with several indices. Then various combinations of slightly different 'a' and 'c' values were used to recalculate the 'd' values so as to obtain better fit with the experimental d-values. It has found that for some peaks several indices had to be assigned as the d-values obtained from these values were too close to be resolved by the diffracting conditions. It was also found that for a few peaks, only one set of indices could be assigned. Other indices which were close to these peaks were at angles far enough to be detected by the diffractometer. Since there were no such indications, they were ignored. Fortunately these two peaks were high intensity peaks, one was of relative intensity 100 (peak 'E')

and corresponds to (330) whereas the other was of relative intensity about 80(peak 'F') and correspond to the indices (3 0 22). The 'E' peak was therefore used to calculate 'a' and 'F' peak to calculate 'c'. The eight prominent, high intensity peaks were identified by A, B, C, D, E, F, G and H. The indexing of these peaks of alloy 8-o-4 is shown in Table 4.1.

A similar table of the alloy containing the same composition but annealed at a lower temperature and quenched from the same are shown in Table 4.2.

The diffractometer tracings of alloys 9-w-5 and 10-w-5 are shown in Figure 4.3 and that of 11-w-5 and 11-w-53 are shown in Figure 5.5.

Lattice Parameters of δ-phase:

The lattice parameters were obtained from the diffractometer tracings in the manner described above. In order to test the reproduciability of these results several measurements were taken with separate samples of the same alloy. Also alloy samples of same composition but heat treated separately under the same conditions (e.g. sample number 11-o-5 and 11-w-5) were also examined. All these data on 'a' and 'c' are listed in Table 4.3. This table also lists the average values of 'a' and 'c'. The scatter in this values are also included in the table. The ratio of the c/a is also included in this.

Table 4.1.   X-ray Diffraction Data of Alloy 8-o-4.

Peak identification number	Relative intensity (I/I_o)	2θ	$d_{experimental}$ (Å)	Possible indices (h k l)	Selected indices of the peaks
A	33	52.075	2.2052	5 0 3 3 2 13	5 0 3 3 2 13
B	44	52.353	2.1943	5 0 4 4 0 16 2 0 14 4 1 11	5 0 4 4 0 16
C	41	53.225	2.1609	4 1 12 5 0 6 3 2 14	4 1 12 5 0 6 3 2 14
D	31	53.455	2.1523	3 1 19	3 1 19
E	100	53.887	2.1363	3 3 0	3 3 0
F	79	54.135	2.1273	3 3 2 3 0 22	3 0 22
G	55	54.385	2.1182	2 0 25 3 2 15 5 0 8	3 2 15
H	35	54.990	2.0970	4 2 0 5 0 9 4 2 1 3 1 20	5 0 9 4 2 1 3 1 0

Table 4.2.   X-ray Diffraction Data of Alloy 8-w-43.

Peak identification number	Relative intensity (I/I_0)	2θ	$d_{experimental}$ (Å)	Possible indices (h k l)	Selected indices of the peaks
A	39	52.075	2.2052	5 0 3 3 2 13	5 0 3 3 2 13
B	55	52.365	2.1938	5 0 4 4 0 16 2 0 24 4 1 11	5 0 4 4 0 16
C	46	53.195	2.1620	4 1 12 5 0 6 3 2 14	4 1 12 5 0 6 3 2 14
D	38	53.415	2.1538	3 1 19	3 1 19
E	100	53.850	2.1377	3 3 0	3 3 0
F	89	54.155	2.1265	3 3 2 3 0 22	3 0 22
G	56	54.358	2.1192	2 0 25 3 2 15 5 0 8	3 2 15
H	40	54.975	2.0972	4 2 0 5 0 9 4 2 1 3 1 20	5 0 9 4 2 1 3 1 0
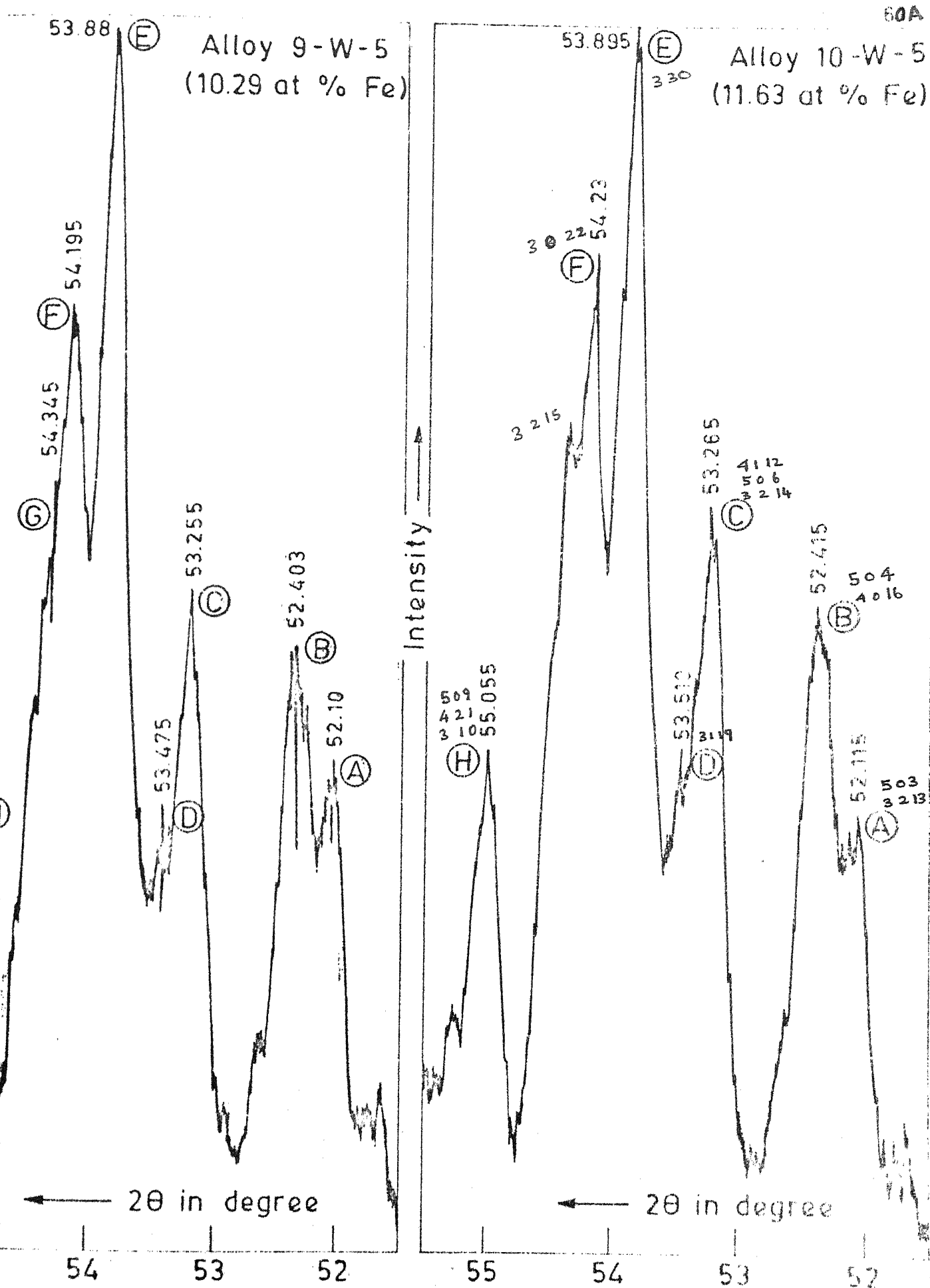
Fig. 4.3. Diffraction Patterns.

Table 4.3. Variation of Unit Cell Parameters of δ-phase of Fe-Zn System with Composition and Heat Treatment (Measured at 26°C).

Compos-ition at % Fe	Temper-ature from which the sample is quenched (°C)	Sample identifi-cation number	Measured value of 'a' (10^{-10} m)	Average value of 'a' (10^{-10} m)	Measured value of 'c' (10^{-10} m)	Average value of 'c' (10^{-10} m)	Specific volume of unit cell (10^{-30} m^3) ($V = a^2c \sin 60°$)	c/a
9.24	473	8-o-4	12.8178 12.8207	12.8193±0.0015	57.1967 57.1992	57.1980±0.0013	8140.29±1.91	4.4619
	350	8-w-43	12.8260 12.8262	12.8261±0.0001	57.1497 57.1436	57.1466±0.0031	8141.61±0.44	4.4555
10.29	552	9-o-55	12.8216 12.8240	12.8228±0.0012	57.0794 57.0900	57.0847±0.0053	8128.61±1.52	4.4518
	552	9-w-5	12.8194 12.8229	12.8211±0.0018	57.1060 57.1222	57.1141±0.0081	8130.65±2.28	4.4547
	350	9-w-53	12.8271 12.8284	12.8278±0.0007	57.1036 57.1094	57.1065±0.0029	8138.05±0.93	4.4518
10.94	567	9.5-55(I)	12.8193	12.8193	57.0697	57.0697	8122.03	4.4519
	567	9.5-5.5(II)	12.8194 12.8196	12.8195±0.0001	57.0915 57.1070	57.0993±0.0078	8126.50±1.11	4.4541
	350	9.5-53	12.8205 12.8218	12.8212±0.0007	57.0455 57.0368	57.0411±0.0044	8120.37±0.89	4.4490

Table 4.3. (continued)

Composition at % Fe	Temperature from which the sample is quenched (°C)	Sample identification number	Measured value of 'a' Å (10⁻¹⁰ m)	Average value of 'a' Å (10^{-10} m)	Measured value of 'c' Å (10^{-10} m)	Average value of 'c' Å (10^{-10} m)	Specific volume of unit cell Å³ (10^{-30} m³) ($v = a^2c \sin 60°$)	c/a
11.63	552	10-p-5	12.8062 12.8042	12.8052±0.0010	57.0406 57.0318	57.0362±0.0044	8099.42±1.27	4.4541
	552	10-w-5	12.8161 12.8141	12.8151±0.0010	57.0624 57.0682	57.0653±0.0029	8116.09±1.27	4.4530
12.67	552	11-p-5	12.8029 12.8042 12.8031	12.8034±0.0005	57.0899 57.0899 57.0633	57.0742±0.0104	8102.54±1.48	4.4577
	555	11-w-5	12.8029 12.8031 12.7998	12.8019±0.0014	57.1058 57.0995 57.1070	57.1041±0.0030	8104.88±1.77	4.4606
	350	11-w-53	12.7853 12.7877	12.7865±0.0012	57.0211 57.0390	57.0300±0.0069	8074.90±1.52	4.4602

Conditions limiting possible reflections for monoclinic structure[30] with a cell symmetry c2/m:

$$h \, k \, l \, : \quad h + k = 2n$$

$$h \, o \, l \, : \quad h = 2n$$

$$o \, k \, l \, : \quad k = 2n$$

Using equation (4.6) and the values of a, b, c and of P.J. Brown, different values of 'd' for all the combinations of h, k and l in the 2θ range 18° to 160° were obtained by the computer program (Appendix 2). The h value is varied from -10 to 10 and k and l are varied from 0 to 10. The experimentally determined values of 'd' of 6.1 wt % Fe were compared with the calculated values and the possible values of h, k and l are noted. These are checked for extinct rules and finally the (h k l) value are allotted to the different peaks in the chart.

In order to obtain values of a, b, c and more accurately, equation (4.6) may be rewritten in the following manner,

For (h k o) type of indices

$$\left(\frac{1}{d^2 k^2}\right) = \left(\frac{h^2}{k^2}\right) \cdot \left(\frac{1}{a^2 \sin^2 \beta}\right) + \frac{1}{b^2} \tag{4.7}$$

Similarly for (h o l) types of indices,

$$\left(\frac{1}{l^2 d^2} - \frac{h^2}{l^2 a^2 \sin^2 \beta}\right) = \frac{1}{c^2 \sin^2 \beta} - \left(\frac{2 \cos \beta}{a^2 \sin^2 \beta \cdot c^2 \sin^2 \beta}\right) \left(\frac{h}{l}\right) \tag{4.8}$$

All the d values corresponding to (h k o) type of planes were selected and $(\frac{1}{d^2 k^2})$ was plotted against $(\frac{h^2}{k^2})$. This is shown in Figure 4.1. The slope of the straight line which resulted from this plot gave the value of $a^2 \sin^2 \beta$ and the intercept gave the value of b^2. Then all the d-values of planes having indices (h o l) were selected and $(\frac{1}{l^2 d^2}) - (\frac{h^2}{l^2 a^2 \sin^2})$ was plotted against (h/l). This is shown in Figure 4.2. The intercept of this line gave $c^2 \sin^2 \beta$ and the slope gave 'β'. Knowing 'β', 'a' and 'c' were calculated. These values are given below:

$$a = 13.3894 \text{ Å}$$
$$b = 7.6249 \text{ Å}$$
$$c = 5.0057 \text{ Å}$$
$$\beta = 126°50' .$$

4.3. Diffraction Patterns Due to Alloys Containing 7.68 at % Fe and 16.01 at % Fe:

Experimentally determined 'd' values of 7.68 at % Fe were compared with those of 7.07 at % Fe and 9.24 at % Fe and it was found that the alloy containing 7.68 at % Fe has diffraction peaks belonging to both γ and δ phases. Some peaks are exclusively due to γ or δ phase and others are due to the overlapping of peaks of both γ and δ suggesting that 7.68 at % Fe alloys contains two phases γ and δ. Because of overlapping and poor resolution, it was not possible to determine the lattice parameters of the co-existing γ and δ phases.
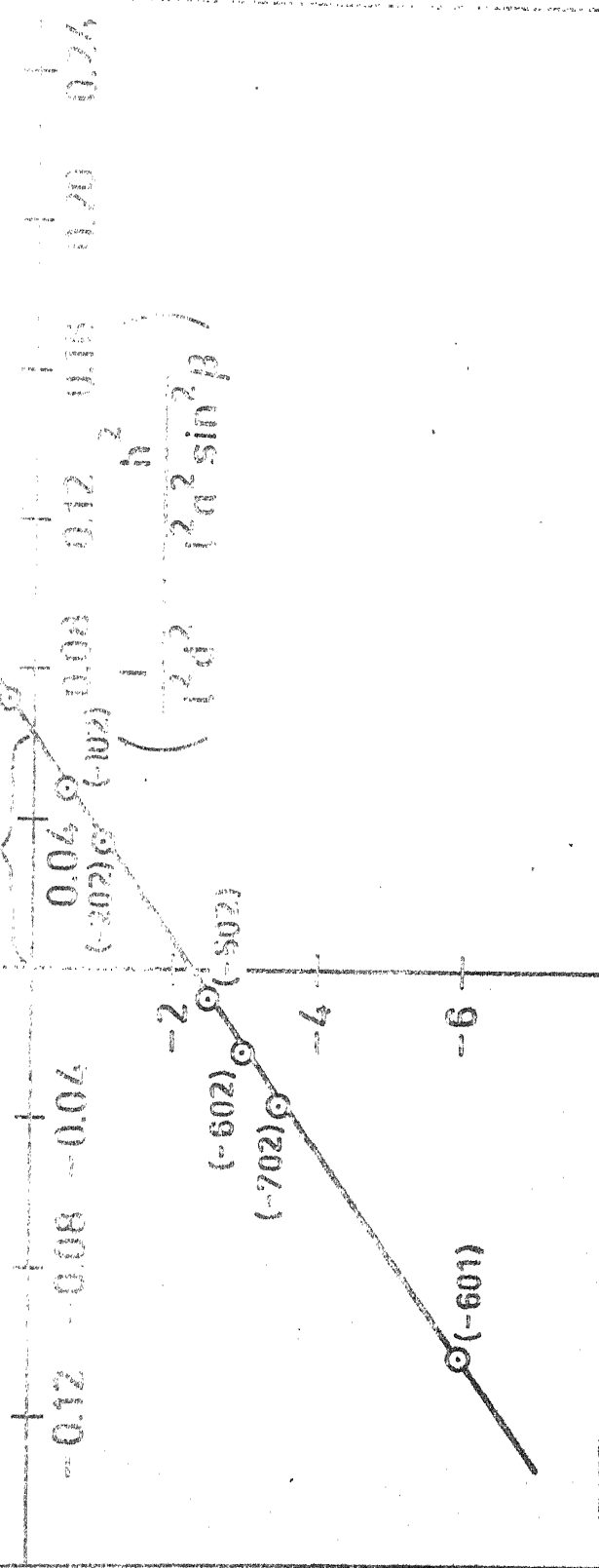
Fig. 4.2. Lattice parameter determination of the ζ -phase of Fe-Zn system.
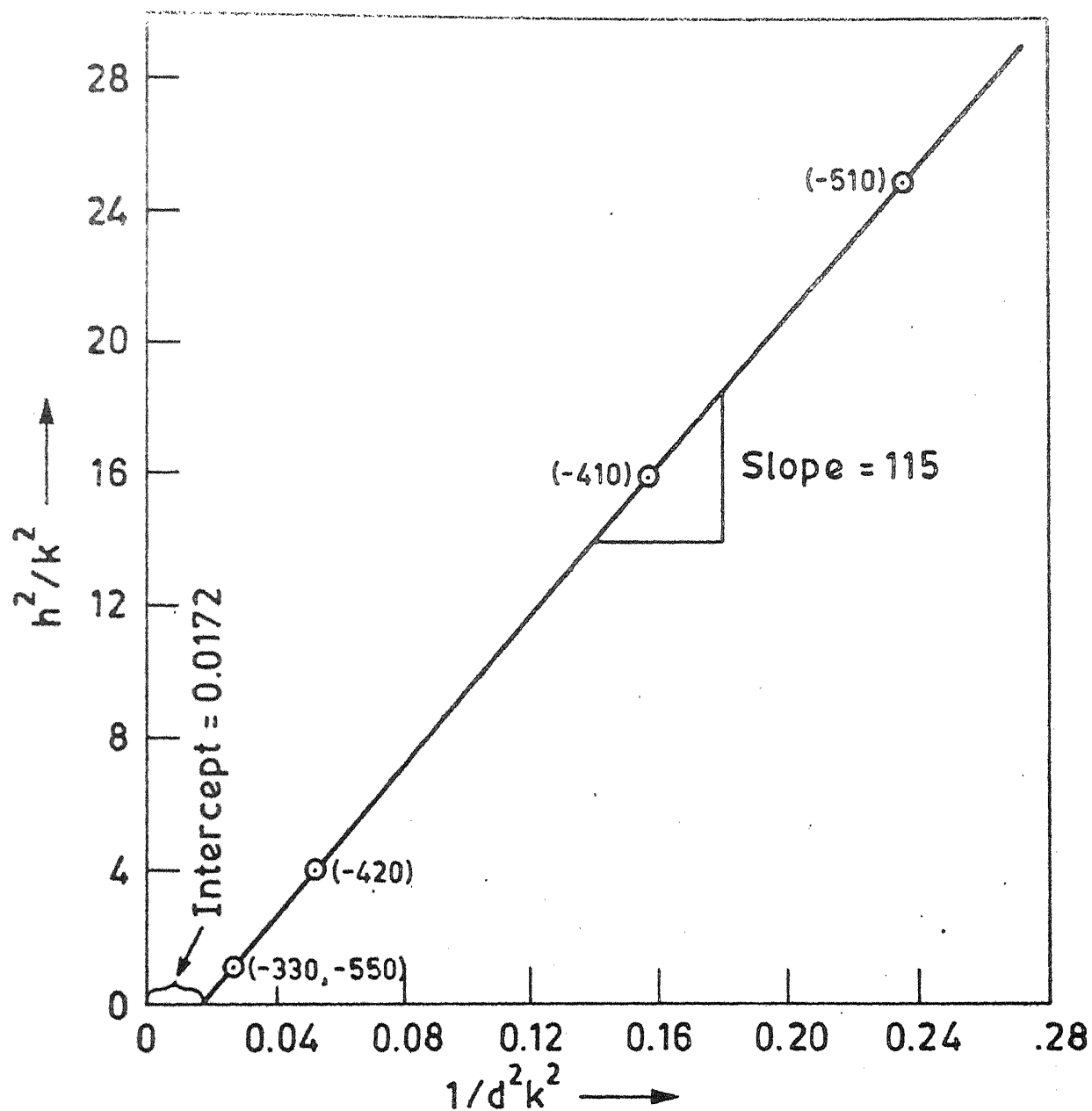
Fig. 4.1. Lattice parameter determination of the ζ phase of Fe - Zn system.

Diffraction patterns of 16.01 at % Fe alloys contained reflections due to δ phase and Γ phase in (14-w-605). Those due to δ and Γ₁ were present in (14-o-550), (14-o-350) and (14-o-475).

4.4. Density Measurements:

The density of the alloy powders were calculated in the following manner:

Weight of the glass tube + wire in air = w_1 gms

Weight of the glass tube + wire + samples in air = w_3 gms

Weight of the samples in air = $(w_3 - w_1) = w_A$ gms

Weight of the glass tube + wire in liquid = w_2 gms

Weight of the glass tube + wire + samples in liquid = w_4 gms

Weight of the samples in liquid = $(w_4 - w_2) = w_L$ gms

Density of the vacuum pump oil at the temperature of the measurement of density, T°C = $(\rho_{oil})_T$ gms/cc

∴ Density of the sample at temperature, T°C

$$= \frac{w_A}{w_A - w_L} \times (\rho_{oil})_T \ \text{gms/cc}$$

$$= \frac{(w_3 - w_1) \times (\rho_{oil})_T}{(w_3 - w_1) - (w_4 - w_2)} \ \text{gms/cc}$$

For accurate density measurements of alloys, the density of the liquid (rotary pump oil) has to be determined accurately. The density of the liquid was measured five times

at 31°C, twice at 29.5°C and 30°C by an imported picnometer whose volume is 10 ml at 20°C. The results were given in Table 4.4.

Table 4.5 gives the measured density values of the Fe-Zn alloys in the -phase. Some alloys (10-w-5, 11-w-5) are repeated three times and values of density obtained were consistent.

All these measurements were made at atmospheric pressure of about 70.2 cm of mercury and at 29.5, 30 or 31°C.

Under these conditions, the density of air[31] at

        29.5°C is 0.001078 gms/cc

        30°C is 0.001076 gms/cc

and   31°C is 0.001072 gms/cc.

It may be noted that the correction in the density of alloys due to air density is small.

Table 4.4   Density of Oil Used for Density Measurements of Alloys.

Testing temperature 'T' (°C)	Weight of empty picnometer (gms)	Weight of the picnometer with oil (gms)	Density of the oil 'ρ' (gms/cc)	Average density 'ρ_T' (gms/cc)
29.5	12.86791	21.67112	0.880321	0.880316 ± 0.000005
	12.86796	21.67107	0.880311	
30.0	12.86387	21.66680	0.880293	0.880301 ± 0.000008
	12.86396	21.66705	0.880309	
31.0	12.86495	21.66991	0.880254	0.880266 ± 0.000028
	12.86160	21.66658	0.880256	
	12.86483	21.66984	0.880259	
	12.86315	21.66851	0.880294	
	12.86463	21.66962	0.880267	

Table 4.5.   Density of Alloys as a Function of Composition and Heat Treatment.

Composition at % Fe	Sample identification number	Number of times expt. repeated	Temperature (T°C)	W_1 gms	W_2 gms	W_3 gms	W_4 gms	Density at T°C	Average density
9.24	8-o-4	(1)	29.5	2.11231	1.29627	3.37413	2.40427	7.22143	
	8-w-43	(1)	30.0	2.11249	1.29632	3.54095	2.55052	7.21608	
10.29	9-o-55	(1)	30.0	2.11903	1.30336	3.43151	2.45628	7.24102	
	9-w-5	(1)	30.0	2.11897	1.30314	3.23670	2.28499	7.24123	7.24131
		(2)	31.0	2.11846	1.30323	3.23429	2.28342	7.24138	$\pm$0.00007
	9-w-53	(1)	29.5	2.11894	1.30338	3.21659	2.26752	7.23750	
10.94	9.5-55 (I)	(1)	30.0	2.11895	1.30336	3.17108	2.22769	7.24719	
	9.5-55 (II)	(1)	29.5	2.11883	1.30323	3.23245	2.28158	7.24727	
	9.5-53	(1)	30.0	2.11901	1.30329	3.21930	2.27002	7.25207	
11.63	10-w-5	(1)	31.0	2.11919	1.30343	3.61355	2.61683	7.26920	7.26860
		(2)	31.0	2.11431	1.29817	3.60219	2.60586	7.26861	$\pm$0.00040
		(3)	30.0	2.11241	1.29632	3.34862	2.38280	7.26800	
12.67	11-w-5	(1)	31.0	2.11915	1.30363	3.15540	2.21487	7.29682	7.29638
		(2)	31.0	2.11431	1.29825	3.02162	2.09609	7.29583	$\pm$0.00037
		(3)	30.0	2.11434	1.29820	2.98680	2.06540	7.29648	
	11-w-53	(1)	31.0	2.11444	1.29821	2.45077	1.59407	7.31554	7.31550
		(2)	31.0	2.11831	1.30318	2.45073	1.59560	7.31545	$\pm$0.00004

CHAPTER   V

DISCUSSION

5.1.   Reproducibility of the Data:

The lattice parameters have been measured several times in case of each specimen at different times. Also samples taken from the same alloy and heat treated separately under same conditions have been used for lattice parameter measurements. It would be noted from Table 5.1 that the scatter in 'a' value of all the results is only about 1.5 in 13,000 i.e., 0.012%. Similarly the scatters in 'c' values is about 1.0 in 6,000 i.e., 0.018%. These low scatters and the reproducibility of results suggests that the data are highly reliable.

The density measurements have also been repeated several times in case of a number of alloys. These show that the density values are also reproducible to about 4 in 73,000 i.e., 0.005%. The accurate density measured by J.O. Betterton and William Hume-Rothery[20] also lay between 1 part in 4,000 and 1 part in 30,000. The density of the alloy are plotted against composition in Figure 5.3.

The data which have been derived from above measurements viz. specific volume of the unit cell and the number of atom per unit cell also contain errors due to the scatter in the above data. These errors can be calculated from the following relations.

Table 5.1. Variation of Number of Atoms Per Unit Cell of the δ-phase of Fe-Zn System with Composition and Heat Treatment.

Composition at % Fe	Sample identification number	Average 'a' (Å)	Average 'c' (Å)	Specific volume 'V' (Å³)	Density (gms/cc)	Atomic weight of the alloy	Number of atoms per unit cell 'N'	'N', rounded to the nearest whole number
9.24	8-0-4	12.8178 ±0.0015	57.1980 ±0.0013	8140.29 ±1.91	7.22143	64.4994	548.934	549
	8-w-43	12.8261 ±0.0001	57.1466 ±0.0031	8141.51 ±0.44	7.21608	64.4994	548.616	549
10.29	9-0-55	12.8228 ±0.0012	57.0847 ±0.0053	8128.61 ±1.52	7.24102	64.3994	550.487	550
	9-w-5	12.8211 ±0.0013	57.1141 ±0.0081	8130.65 ±2.28	7.24131 ±0.00007	64.3994	550.647 ±0.154	551
	9-w-53	12.8278 ±0.0007	57.1065 ±0.0029	8138.05 ±0.93	7.23750	64.3994	550.858	551
10.94	9.5-55(I)	12.8193	57.0697	8122.03	7.24719	64.3374	551.041	551
	9.5-55(II)	12.8195 ±0.0001	57.0993 ±0.0078	8126.50 ±1.11	7.24727	64.3374	551.350	551
	9.5-53	12.8212 ±0.0007	57.0411 ±0.0044	8120.37 ±0.89	7.25207	64.3374	551.299	551

Table 5.1 (continued)

Compos- ition at % Fe	Sample identifi- cation number	Average 'a' (Å)	Average 'c' (Å)	Specific volume 'V' (Å³)	Density (gms/cc)	at wt weight of the alloy	Number of atoms per unit cell 'N'	'N', rounded to the nearest whole number
11.63	10-w-5	12.8151 ±0.0010	57.9653 ±0.0029	8116.09 ±1.17	7.26060 ±0.00040	64.2717	552.829 ±0.078	553
	10-o-5	12.8052 ±0.0010	57.9362 ±0.0044	8099.42 ±1.27	--	64.2717	--	--
12.67	11-o-5	12.8034 ±0.0005	57.9742 ±0.0104	8102.54 ±1.43	--	64.1725	--	--
	11-w-5	12.8019 ±0.0014	57.9041 ±0.0030	8101.88 ±1.77	7.29638 ±0.00037	64.1725	555.032 ±0.121	555
	11-w-53	12.7865 ±0.0012	57.9300 ±0.0089	8074.90 ±1.52	7.31550 ±0.00004	64.1725	554.428 ±0.104	554

Specific volume per unit cell (V) $= k_1 a^2 .c$

where k_1 is constant.

Error in 'V' $= dV = k.c.2a.da + ka^2.dc$

$\therefore dV = V(\pm 2 \frac{da}{a} \pm \frac{dc}{c})$

Number of atoms per unit cell (N) $= k_2 . V . \rho$

where k_2 is constant.

Error in N $= dN = N(\pm \frac{dV}{V} \pm \frac{d\rho}{\rho})$

The scatters in V and N calculated on the basis of above relations are listed in Table 5.1. It may be noted that these scatters are also low.

5.2. Comparison with Published Data:

The lattice parameters of δ-phase have been measured by Bastin et al[4] as a function of composition. These data were obtained over a temperature range from 515°C to 660°C. These data have been plotted in Figure 5.1 along with those of ours obtained with samples heat treated at higher temperatures. The figure shows that the variation of lattice parameters with composition is similar in both the cases, although the scatter in Bastin et al's values are much higher. This could be partly because of the range of temperature used by them. But the powder pattern of the δ-phase reported by Bastin et al is similar to that of ours.
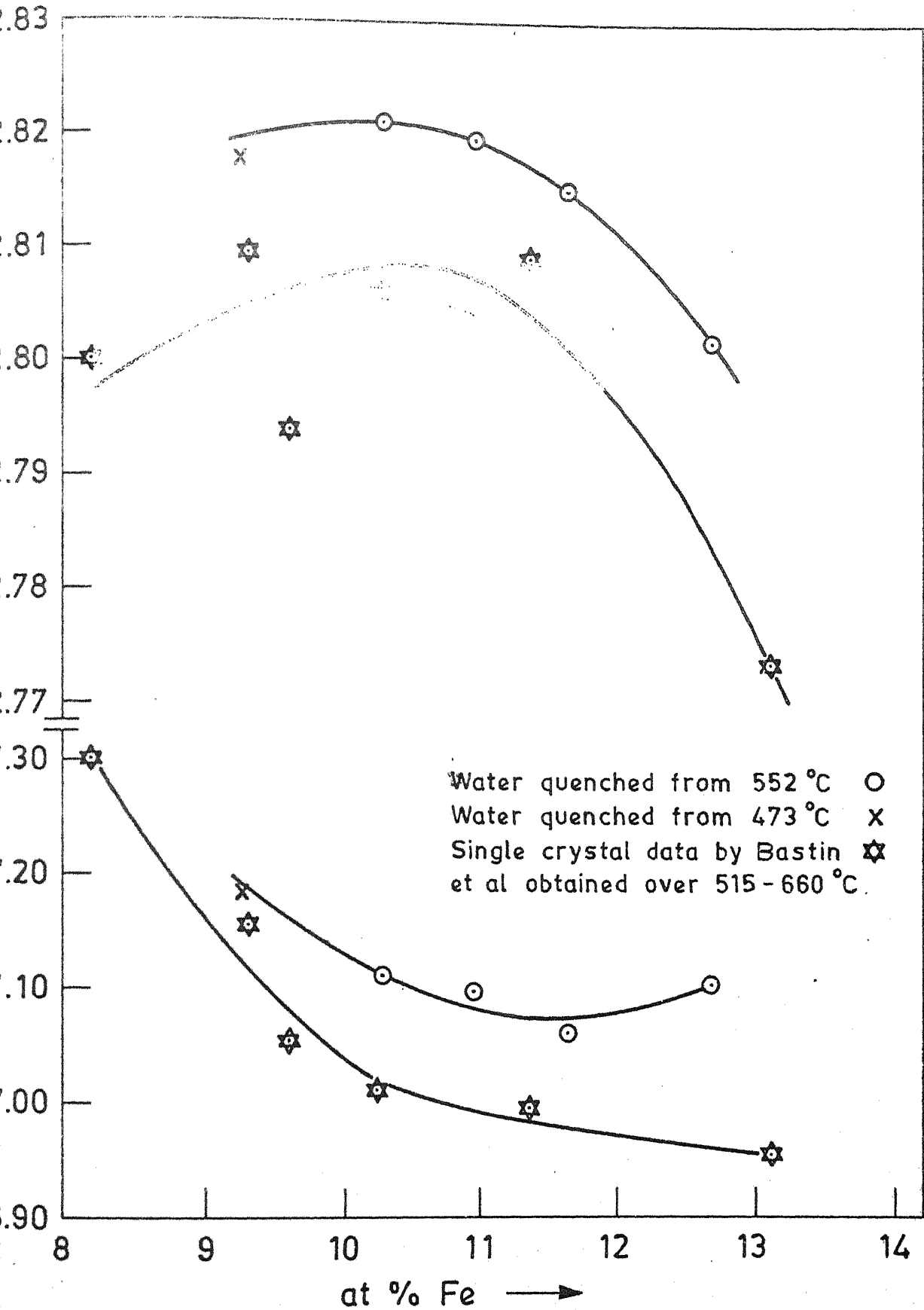
Fig. 1. Comparison of the lattice parameter data for δ-phase of the author with that of Bastin et al.

The legend in the figure reads:

Water quenched from 552 °C ○
Water quenched from 473 °C ×
Single crystal data by Bastin ✪
et al obtained over 515 – 660 °C

The x-axis is labeled "at % Fe ⟶" ranging from 8 to 14.

The lattice parameters of the ζ-phase determined in this investigation are:

$$a = 13.3984 \text{ Å}$$
$$b = 7.6249 \text{ Å}$$
$$c = 5.0057 \text{ Å}$$
$$\beta = 126.83°$$

which compares well with those of Brown   of

$$a = 13.424 \text{ Å}$$
$$b = 7.608 \text{ Å}$$
$$c = 5.061 \text{ Å}$$
$$\beta = 127.3°$$

The powder pattern of ζ-phase has been reported by Gellings et al.[5]. Table 5.2 gives the observed peak positions and the indices determined by us using Brown's proposed unit cell. This table also contains indices reported by Gellings. Some of his proposed indices do not match with those of ours and this is primarily because of poor resolution of peaks of Gellings et al as they have used CuK_α radiation.

There is no accurate density data available on the δ-phase. The value of 7.24 gms per cc given in the literature is close to the measured values.

5.3.   Phases in Iron-Zinc System:

The X-ray data suggests that the 7.07 at % Fe alloy contains a single phase 'ζ'. The 9.24, 10.29, 10.94, 11.63 and 12.67 at % Fe alloys contain a single phase 'δ'. This

Table 5.2.   Comparison of X-ray Powder Pattern of the δ-phase with that of P.J. Gellings et al.

Author's indices (same as that of Brown's)	Experimental values of author		Experimental values of P.J. Gellings et al		P.J. Gellings' indices	Brown's indices
	Relativee intensity	d (Å)	Relative intensity	d (Å)		
0 2 1	10	2.7705	10	2.769	-2 2 1	0 2 1
2 0 1	9	2.5580	2	2.558	-4 0 1	2 0 1
-5 1 1	35	2.5168	11	2.511	3 1 1	-5 1 1
-2 0 2	13	2.4429	27	2.442	-2 0 2	-2 0 2
-1 3 1	11	2.2532	14	2.248	-1 3 1	-1 3 1
-5 1 2	6	2.2311	8	2.228	1 1 2	-5 1 2
-4 2 0	53	2.1897	60	2.188	4 2 0	4 2 0
-3 3 1	100	2.1761	100	2.174	1 3 1	-3 3 1
-1 1 2	70	2.1596	50	2.160	-3 1 2	-1 1 2
2 2 1	82	2.1273	88	2.123	-4 2 1	2 2 1
-6 0 2	39	2.1159	40	2.113	2 0 2	-6 0 2
-4 2 2	45	2.0873	49	2.085	0 2 2	-4 2 2
-5 1 0	60	2.0600	71	2.057	-5 1 0	5 1 0
1 3 1	13	1.9850	15	1.986	-3 3 1	1 3 1
-6 2 1	18	1.9016	44	1.900	4 2 1	-6 2 1
4 0 1	11	1.7863	18	1.787	-6 0 1	4 0 1

(handwritten margin notes: -4 2 1), 601), -2 2 2, (040))

is obvious from the smooth variation of lattice parameters
'c' and densities 'ρ' of these alloys as seen in Figures 5.2
and 5.3.

7.68 at % Fe alloy contains two phases γ_1 and δ at
475°C. The 16.01 at % Fe alloy contains δ and Γ at 605°C,
whereas at 550°C, 475°C and 350°C, it contains δ and Γ_1. So
these results are consistant with the phase diagram which
shows that Γ_1 is unstable above about 550°C and δ is a single
phase material above 550°C. At 350°C, the lattice parameters
of δ phase behave differently which would be discussed on
the following sections.

5.4. Structure of δ -phase:

The δ phase is hexagonal as suggested by others.
However its specific volume decreases with increasing iron
content whereas the density increases with the iron content.
The net result is that the number of atoms per unit cell
remains almost constant as shown in Table 5.1. It is 549 at
the zinc rich end and increases to 555 in the iron rich end.
The increase in the specific volume of the unit cell with
increase in zinc content may be because of the larger size
of the zinc atom.

The Goldsmith atomic diameter of zinc = 2.748 Å

and that of iron   = 2.520 Å

Thus the size of the zinc atom is greater by 8.3%. However,
the decrease in the number of atoms per unit cell is about
$\frac{6}{550} \times 100 \simeq 1.1\%$.
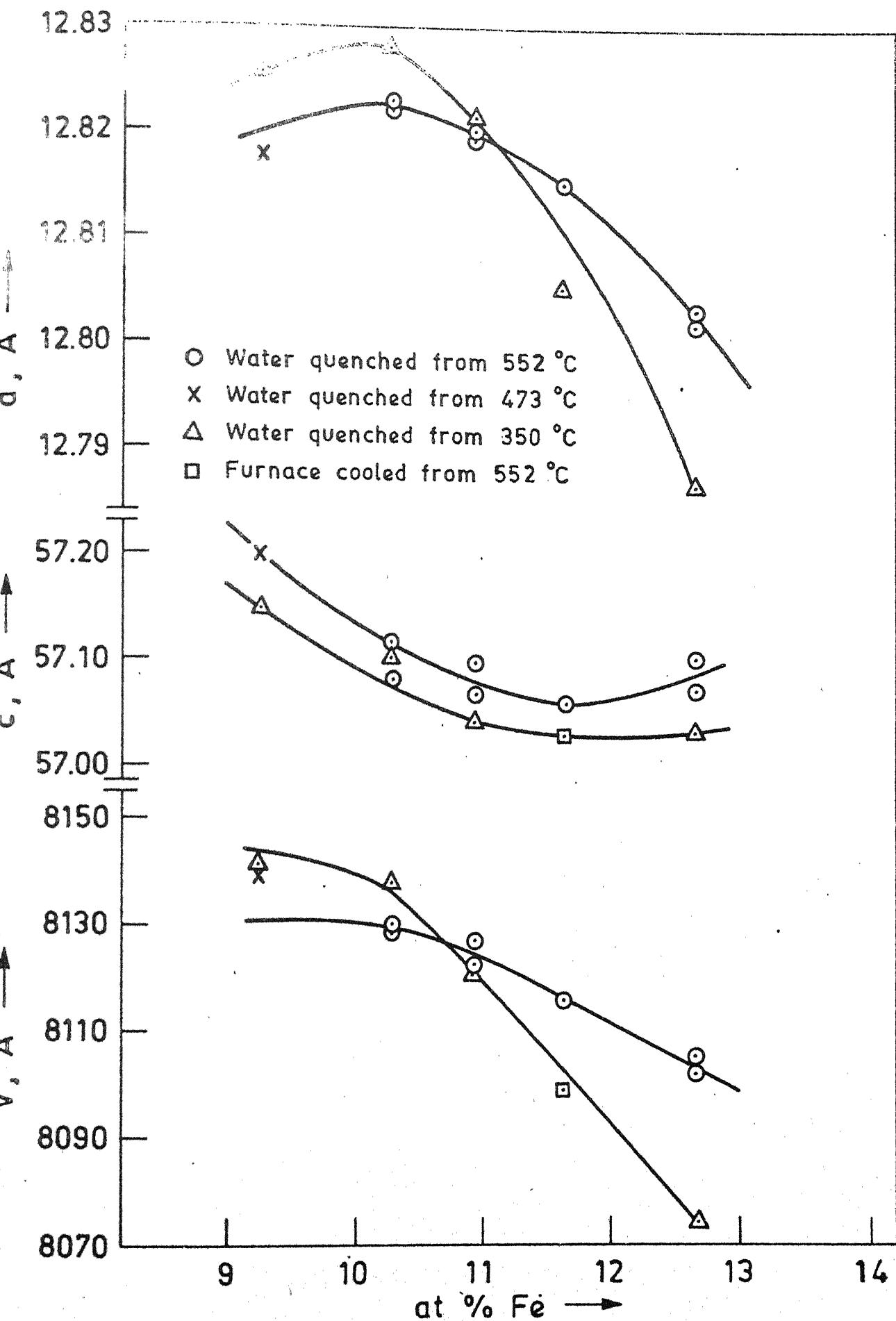
Fig. 5.2. Variation of unit cell parameters of δ-phase system with composition and heat treatment

Legend:
- ○ Water quenched from 552 °C
- × Water quenched from 473 °C
- △ Water quenched from 350 °C
- □ Furnace cooled from 552 °C

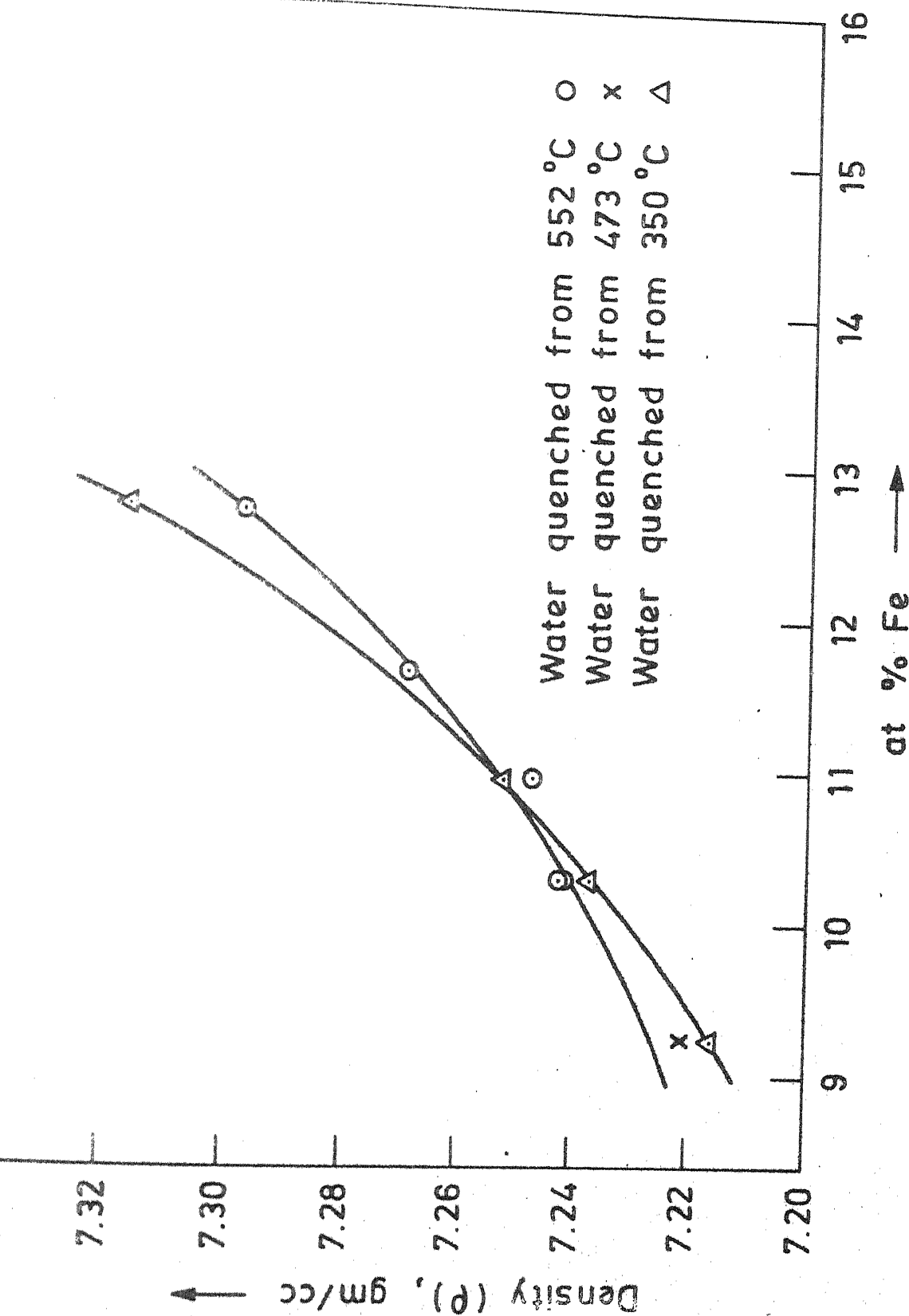Axes:
- x-axis: at % Fe →
- y-axes: a, A →; c, A →; V, A →

Fig. 5.3. Variation of densities of the alloys of δ-phase of Fe-Zn system with composition and heat treatment.

The electron to atom ratio of the δ-phase can be
calculated by assuming that the zinc atom contributes two
electrons and iron contributes zero electrons. The calcula-
tions are shown in Table 5.3. The e/a ratios are plotted
against the atom fraction of Fe in Figure 5.4. It shows the
e/a ratio increases linearly with increasing zinc

The plot of c/a ratio against composition is shown
in Figure 5.4, shows a minimum at about 10.94 at % Fe. This
minimum does not appear to be related to the variation in
e/a ratio.

5.5.   Effect of Low-Temperature Annealing on the Structure of δ-phase :

The alloy specimens annealed at 350°C, show exactly
the same type of diffraction pattern as the samples at higher
temperatures. However, the lattice parameters of the phases
annealed at lower temperature are almost different. The
plots of a, c and specific volume V of high and low temper-
ature specimens are shown in Figure 5.2 which shows that there
is a contraction in the volume of the unit cell of about 0.51%.
This contraction becomes less with decrease in iron content.
Zero at about ~~12.67~~ 10.7 at % Fe. Below that it is slightly
higher. The number of atoms per unit cell however does not
change with heat treatment (Figure 5.4). Thus the number
of atoms per unit cell remains same but the volume contracts.
This can happen due to ordering.

Table 5.3. Calculation of 'e/a' Ratio.

Composition of alloy (at % Fe)	Number of atoms per unit cell (Ref. Table 5.1)	Number of atoms of Fe per unit cell	Number of atoms of Zn per unit cell	e/a
9.21	519	51	498	1.814
10.28	551	57	494	1.793
10.94	551	60	491	1.782
11.63	553	64	489	1.768
12.67	555	70	485	1.748

Example: Calculation of e/a ratio of alloy containing 12.67 at % Fe:

Number of atoms per unit cell = 555

Number of atoms of Fe = $\frac{12.67}{100}$ x 555 = 70.3

= 70

Number of atoms of Zn = (555 - 70) = 485

Number of electrons in the unit cell = 485 x 2 = 970

$\therefore$ e/a = $\frac{970}{555}$ = 1.748 .
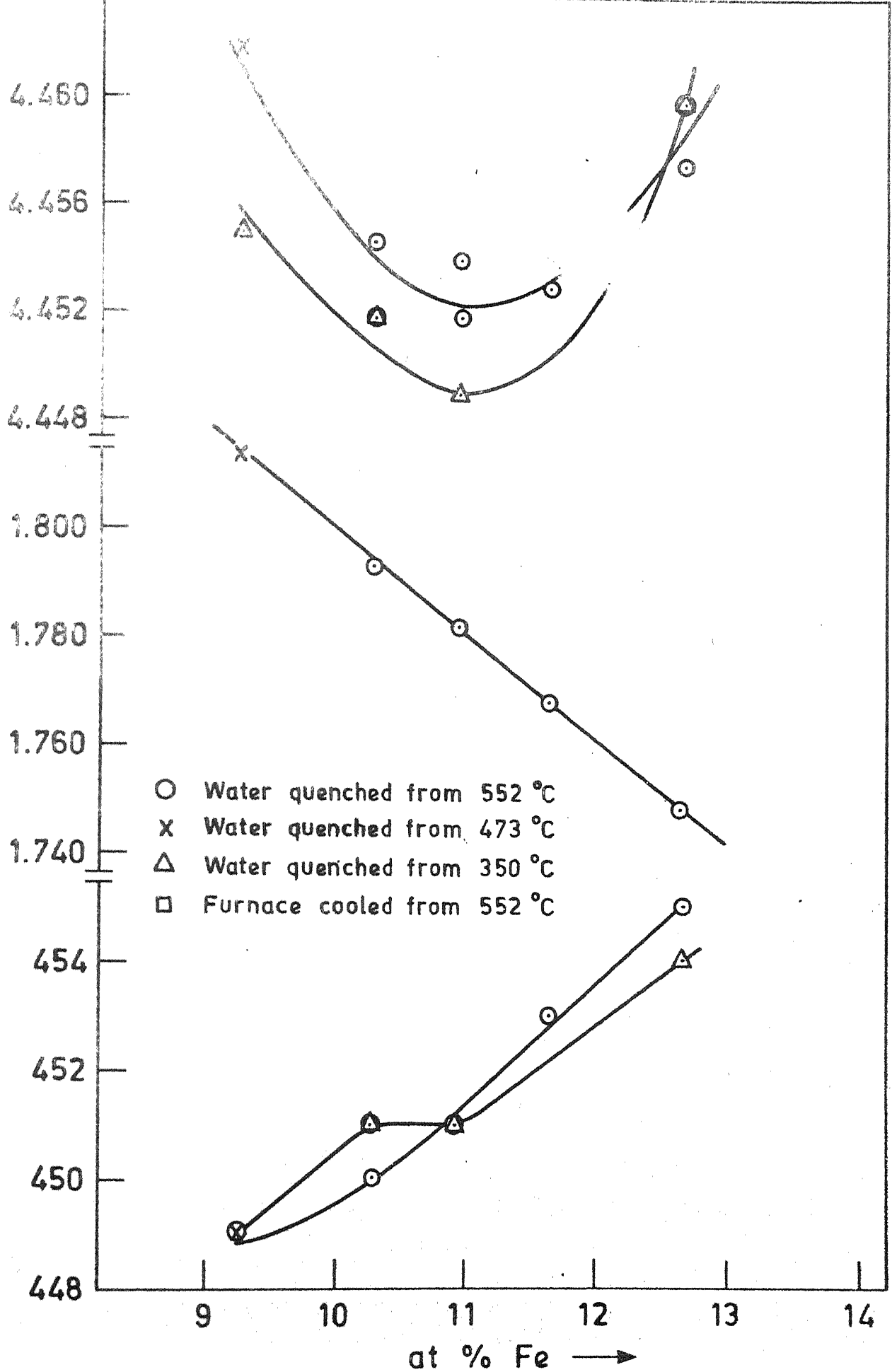
Fig. 5.4. Variation of c/a, e/a and the number of atoms per unit cell (N)
of δ-phase of Fe-Zn system with composition and heat treatment

Legend within figure:

○ Water quenched from 552 °C
× Water quenched from 473 °C
△ Water quenched from 350 °C
□ Furnace cooled from 552 °C

Wright and Goddard[33] studied the ordering of Au_3Cu phase. This phase has face centered cubic structure and its lattice parameter 'a' was decreased from 3.9844 Å to 3.9820 Å with development of order through long annealing at 165°C. The volume of the unit cell has decreased about 0.18% by ordering.

Hirabayashi[34] reports that disordered polycrystalline Au_3Cu phase containing 75.06 at % Au, quenched from 450°C had 'a' = 3.9844 Å whereas ordered Au_3Cu annealed for 4 months at 150°C had 'a' = 3.9810 Å. The decrease in volume of the unit cell is about 0.256%.

In Table 5.4 and in Figure 5.5 the diffraction patterns of 11-w-5 and 11-w-53 are compared. Table 5.4 shows only the major predominant peaks. There are other weak peaks which could not be clearly identified. Therefore the effect of heat treatment of these peaks could not be found. It would be noted that the intensities of the peaks in both the alloys are almost the same but the 'd' values of the peaks of 11-w-53 are consistently lower than those of 11-w-5.

Figure 5.6a shows the possible ordering reaction in the δ-phase. At high temperature it has a disordered structure. On annealing at a lower temperature, the iron rich δ becomes ordered giving rise to greater contraction in volume. As the iron content decreases, the degree of ordering decreases and the contraction becomes zero at about 10.7 at % Fe. When the iron content is decreased further, there is hardly any change in volume.

Table 5.4. Comparison of the Lattice Spacings of the Fe-Zn Alloys Containing 12.67 at % Fe.

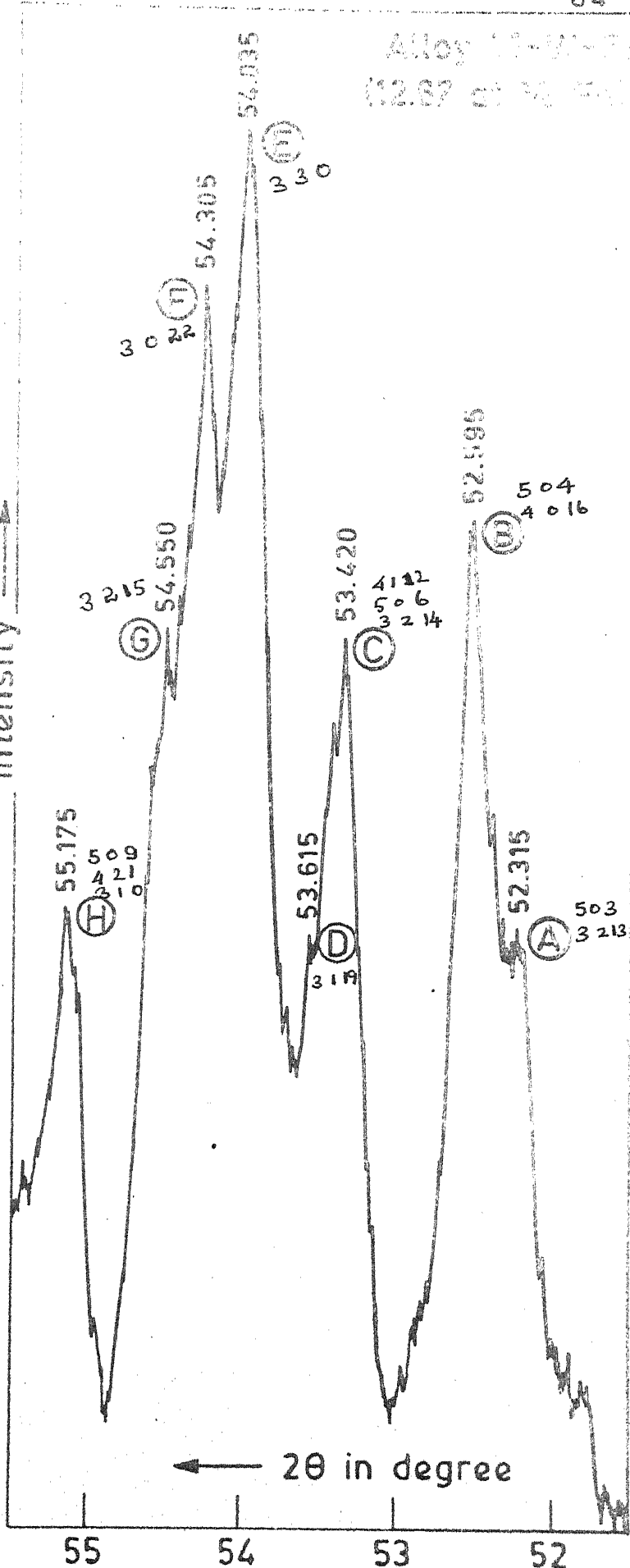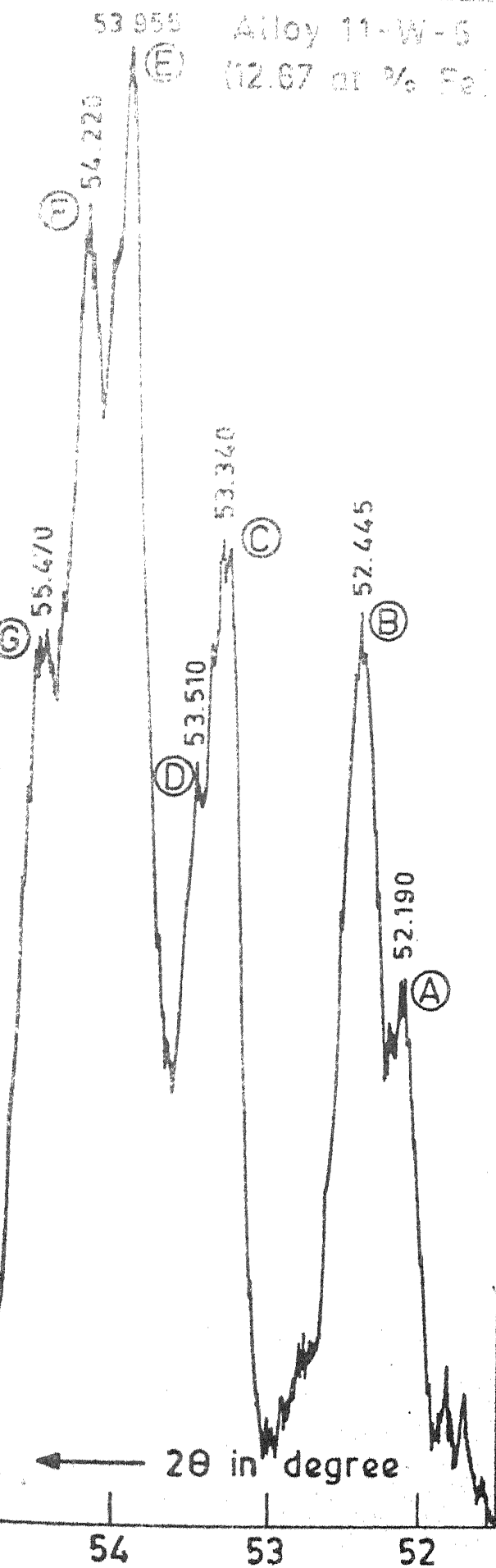| Peak identification number | Alloys | | | | indices |
| | 11-w-5 | | 11-w-53 | | |
	Relative intensity	d (Å)	Relative intensity	d (Å)	(hkl)
A	43	2.2007	42	2.1958	5 0 3 / 3 2 13
B	61	2.1907	72	2.1849	5 0 4 / 4 0 16
C	66	2.1566	64	2.1536	4 1 12 / 5 0 6 / 3 2 14
D	50	2.1502	42	2.1463	3 1 19
E	100	2.1338	100	2.1409	3 3 0
F	88	2.1242	89	2.1211	3 0 22
G	60	2.1152	64	2.1123	3 2 15
H	30	2.0900	44	2.0902	5 0 9 / 4 2 1 / 3 1 0

Fig. 5.5. Diffraction Patterns.

The unusual variation of c/a ratio with composition
as seen in Figure 5.4 can be explained in the following manner:

In Figure 5.4, the c/a ratio steadily decreases upto
about 10.8 at % Fe and reaches a minimum and steadily increases
as the iron content becomes more than 10.8 at % Fe. The 'c'
parameter steadily decreases (Figure 5.4) whereas the 'a' para-
meter remains almost constant upto 10.8 at % Fe. This causes
a steady decrease of c/a ratio upto 10.8 at % Fe, and at higher
iron concentrations, the 'c' remains constant whereas the 'a'
decreases resulting a steady increase of c/a ratio.

The atomic size of zinc is bigger than that of iron.
As the atom percent of iron increases, more and more of zinc
atoms are replaced by the iron atoms. Upto about 10.8 at % Fe,
the zinc atoms are replaced by the iron atoms probably in the
'c' sites (Figure 5.6b), so the length of the 'c' axis in the
unit cell decreases while the length of 'a' axis remain
constant. It is also possible for an exchange of zinc and
iron atoms between 'c' and 'a' axis. More zinc atoms from 'c'
sites are diffusing to 'a' sites and the depleted zinc sites
in the 'c' sites are substituted by the incoming iron atoms
due to the increase in concentration of iron atoms.

At iron concentrations more than about 10.8 at % Fe,
the zinc atoms are replaced by the iron atoms in the 'a' sites
and no substitution taking place in the 'c' axis. Since the
depleting zinc atoms (due to the increase in the concentration
of iron) are replaced by the iron atoms in the 'a' sites,
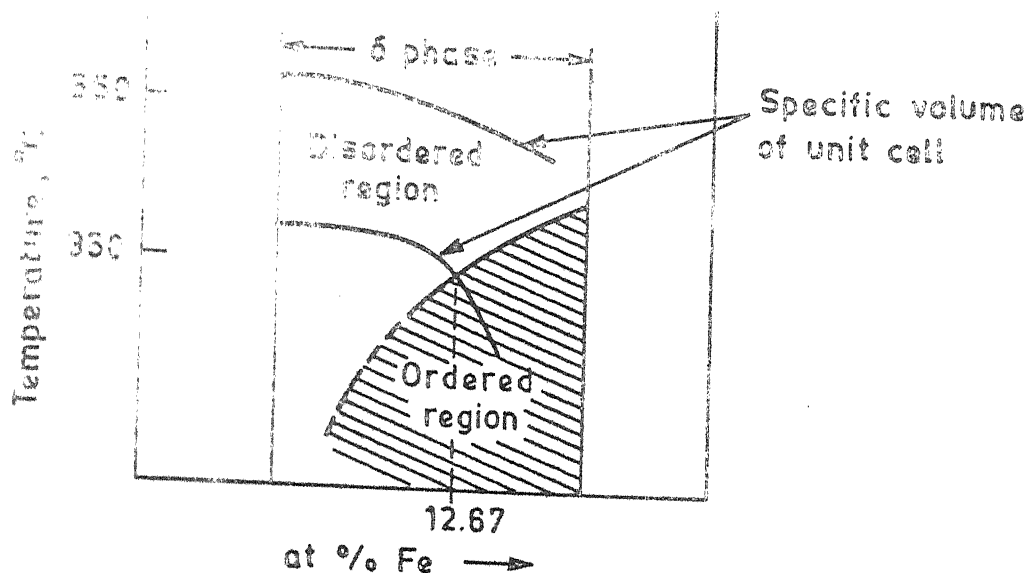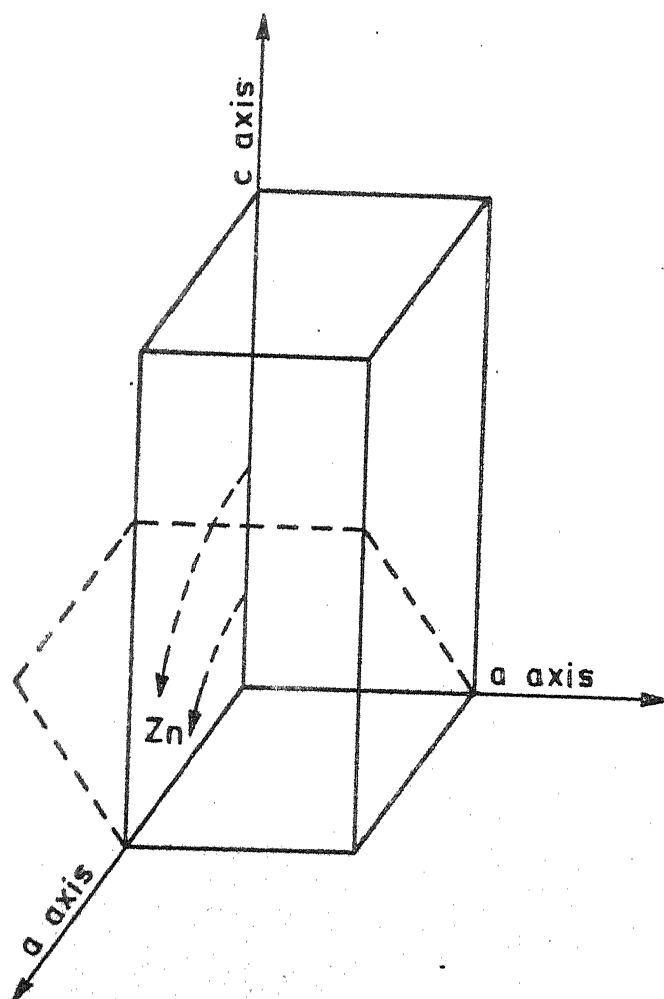
Fig. 5.6c Possible ordering reaction in the δ phase.

Fig. 5.6b. Possible exchange of atoms in the unit
cell of the δ phase.

the 'a' parameter decreases while the 'c' remaining constant. This results in a steady increase of c/a ratio at concentration of iron higher than 10.8 at % Fe.

CHAPTER VI

SUMMARY, CONCLUSION AND SUGGESTIONS FOR FURTHER STUDY

6.1.   Summary and Conclusions:

(1)   Representative specimens of iron-zinc alloys containing 7.07, 7.68, 9.24, 10.29, 10.94, 11.63, 12.67 and 16.01 at % Fe were prepared by melting and annealing at suitable temperatures.

(2)   X-ray diffraction work was carried out on the powders of the alloys of δ-phase of iron-zinc system and unit cell parameters viz. a, c, V, c/a and N were calculated and the variation of these parameters with composition and heat treatment was obtained.

(3)   The γ-phase of the iron-zinc system was indexed and the unit cell parameters were obtained.

(4)   It was found that the 7.68 at % Fe contain both δ and ζ phases.

(5)   The high temperature 16.01 at % Fe alloys of iron-zinc system contain both δ and Γ phases and the low temperature 16.01 at % Fe contain δ and Γ_1 phases.

(6)   The density measurements were carried out on the alloys of δ-phase and the variation of the density with composition and heat treatment were obtained.

(7)   The possibility of order-disorder transformation at 12.67 at % Fe in the δ-phase was discussed.

6.2.   Suggestions for Further Study:

The further study on the order-disorder transformation of the δ-phase may be carried out in the following lines:

(1)   The high temperature and low temperature alloys of δ-phase can be examined under the Transmission Electron Microscope and the domain structure, selected area diffraction and extra spots if any because of ordering can be observed.

(2)   Differential thermal analysis can be carried out on the alloys of δ-phase and the transformation temperature of different phases can be studied by the heat effects.

(3)   Conductivity measurements, if can be conducted, can through light on this.

REFERENCES

1. J. Mackowiak and N.R. Short, International Metals Reviews. 1979, No. 1.

2. J. Schramm, Z. Metallkde. 30 (1938) 131.

3. M. Ghoniem and M. Lohberg, Metall. 26 (1972) 1026.

4. G.F. Bastin, F.J.J. Van Loo, and G.D. Rieck, Z. Metallkde. 68 (1977) 359.

5. P.J. Gellings, E.W. de Bree and G. Gierman, Z. Metallkde. 70 (1979) 315.

6. S.W.K. Morgan, Zinc and Its Alloys, Industrial Metal Series (1977).

7. H. Buhler, G. Jackl, L. Meyer, and S. Baumgartl, Microchim. Acta, Suppl. IV (1979) 75.

8. C. Allen and J. Mackowiak, Corrosion Sci. 3 (1963) 87.

9. A. Hershman, 7th Internat. Galvan. Conf. (1969) 189.

10. G.F. Bastin, F.J.J. Van Loo, and G.D. Rieck, Z. Metallkde. 67 (1976) 695.

11. P.J. Gellings, E.W. de Bree, and G. Giermar, Z. Metallkde. 70 (1979) 312.

12. C. Allen and J. Mackowiak, J. Inst. Met. 91 (1962-63) 369.

13. D. Horstman and F.K. Peters, Proceedings of 9th Internat. Galvan. Conf. (1970) 75.

14. J. Mackowiak and N.R. Short, Corros. Sci. 16 (1976) 519.

15. H. Bablik, F. Gotzl, and F. Halla, Z. Metallkde. 8 (1938) 249.

16. F. Gotzl, F. Halla, and J. Schramm, Z. Metallkde. 33 (1941) 375.

17. P.J. Brown, Acta Cryst. 15 (1962) 608.

18. G.F. Bastin and F.J.J. Van Loo, Z. Metallkde. 69 (1978) 540.

19. G.F. Bastin, F.J.J. Van Loo, and G.D. Rieck, Z. Metallkde. 65 (1974) 656.

20. E.C. Ellwood, J. Inst. Met. LLXXX (1951-52) 217.

21. J.O. Betterton and William Hume-Rothery, J. Inst. Met. LLXXX (1951-52) 459.

22. A.K. Jena, Unpublished Work in Technical University of Berlin, West Germany.

23. Operator's Manual Model IL 751 AA/AE Spectrometer, Instrumentation Laboratory, Inc.

24. G.F. Kirkbright and M. Sargent, 'Atomic Absorption and Fluorescence Spectroscopy' (1974), Academic Press.

25. Atomic Absorption Methods Manual, 1, 'Flame Operations' Instrumentation Lab. Inc.

26. W. Bygrare, P. Trado and J. Lambert, 'Accelerator Nuclear Physics'.

27. S. Sen, C.K. Mehta et al, 'Trace Element Analysis Using Proton Induced X-ray Emission', Technical Report VDG/15/79, I.I.T. Kanpur.

28. H.P. Clug and L.E. Alexander, 'X-ray Diffraction Procedures'.

29. B.D. Cullity, 'Elements of X-ray Diffraction'.

30. International Tables for X-ray Crystallography, 1, Symmetry Groups, 95.

31. Handbook of Chemistry and Physics, 45th edition, p. F3.

32. W.B. Pearson, 'Handbook of Lattice Spacings and Structures of Metals - 2, 8 (1967).

33. P. Wright and K.F. Goddard, Acta Met. 7 (1959) 757.

34. M. Hirabayashi, J. Phys. Soc. Japan, 14 (1959) 262.

```
******************************************************************************
     PROGRAM FOR INDEXING OF THE HEXAGONAL CRYSTAL STRUCTURE.
     AND CALCULATION OF 'd' SPACINGS.
******************************************************************************

     REAL K1,K,AA
     DIMENSION D(1000),IH(1000),IK(1000),IL(1000),AKM(1000),THE(1000)
     OPEN(UNIT=1,DEVICE='DSK',FILE='DON.DAT')
     READ(1,*)A,C,WHIGH,ELOW
     I=1
     DO 10 I1=1,30
     DO 10 I2=1,30
     DO 10 I3=1,30
     H1=I1-1
     K1=I2-1
     L1=I3-1
     IF((H1+K1+L1).EQ.0.) GO TO 10
     D11=(1.33333*(H1*H1+H1*K1+K1*K1)/(A*A))+(L1*L1)/(C*C)
     D12=1.0/D11
     D13=SQRT(D12)
     D1=ABS(D13)
     T1=0.96705/D1
     AKM(I)=H1*T1
     T2=SQRT(ABS(1.-T1*T1))
     T3=T1/T2
     T=ATAN(T3)
     T4=T*180./3.141592
     THE(I)=2.*T4
     D(I)=D1
     IF(D1.GT.WHIGH) GO TO 10
     IF(D1.LT.ELOW) GO TO 10
     IH(I)=H1
     IK(I)=K1
     IL(I)=L1
     I=I
     I=I+1
  10 CONTINUE
     MAX=0.
     DO 30 KN=1,14
     DA=0.
     DO 20 J=1,14
     IF(D(J).LE.DA) GO TO 20
     DA=D(J)
     LS=I
  20 CONTINUE
     IF(DA.EQ.MAX) GO TO 30
     MAX=DA
     WRITE(IK(LS),IH(LS),IL(LS),DA,AKM(LS),THE(LS)
     FORMAT(1X,3(I2,2X),F10.5,2X,F10.4,2X,F10.2)
     CONTINUE
     STOP
     END
```

```
***********************************************************************
    PROGRAM FOR INDEXING THE MONOCLINIC CRYSTAL STRUCTURE
    TO OBTAIN THE 'd' SPACINGS.
    ( THE VALUES OF 'a','b','c' AND 'β' ARE USED. )
***********************************************************************

      READ (11,4) A,B
      DIMENSION D(1000),IH(1000),IK(1000),IL(1000),AKM(1000),THE(1000)
      OPEN(UNIT=21,DEVICE='DSK',FILE='NEW.DAT')
      READ (21,4) F,HIGH,FLOW
      I=1
      DO 10 I1=1,21
      DO 10 I2=1,11
      DO 10 I3=1,11
      H1=I1-11
      K1=I2-1
      L1=I3-1
      IF((H1+K1+L1).EQ.0.) GO TO 10
      D11=0.002/695*H1*H1+0.0172706*K1*K1+0.0616985*L1*L1+
     1 0.02919191*H1*L1
      D12=1./D11
      D13=SQRT(D12)
      D1=ABS(D13)
      T1=0.96/985/D1
      AKM(I)=H1*T1
      T2=SQRT(ABS(1.-H1*T1))
      T3=H1/T2
      T=ATAN(T3)
      T4=T*180./3.141592
      THE(I)=2.*T4
      D(I)=D1
      IF(D1.GT.HIGH) GO TO 10
      IF(D1.LT.FLOW) GO TO 10
      IH(I)=H1
      IK(I)=K1
      IL(I)=L1
      T4=1
      I=I+1
   10 CONTINUE
      MAX=0.
      DO 30 KM=1,14
      DA=0.
      DO 20 J=1,14
      IF(D(J).LE.DA) GO TO 20
      DA=D(J)
      LS=J
   20 CONTINUE
      D(LS)=0.
      IF(DA.EQ.MAX) GO TO 30
      MAX=DA
      TYPE 40,IH(LS),IK(LS),IL(LS),DA,THE(LS),AKM(LS)
      PRINT 40,IH(LS),IK(LS),IL(LS),DA,THE(LS),AKA(LS)
   40 FORMAT(1H0,5X,3(I3,1X),F11.5,3X,F11.3,5X,F10.5)
   30 CONTINUE
      STOP
      END
```

```
*************************************************************************

    GENERAL PROGRAM FOR INDEXING ALL CRYSTAL STRUCTURES.

    DETERMINATION OF INTERPLANAR SPACING CORRESPONDING
    TO (HKL) VALUES FOR DIFFERENT PHASES IN IRON-ZINC ALLOYS

*************************************************************************

DIMENSION IL(15),IH(7),IK(71),D(15,7,71)

-------------------------------------------------------------------------

1)    THE ALPHA,BETA,GAMMA VALUES ARE GIVEN FOR A PARTICULAR
      HEXAGONAL SYSTEM.
      THE SAME PROGRAM CAN BE USED FOR ANY OTHER SYSTEM ONLY
      BY CHANGING THEIR VALUES.
2)    THE VALUES OF a,b,c ARE TO BE GIVEN VIA TERMINAL. WHEN
      YOU START EXECUTING THE COMPUTER WILL FIRST WANT TO KNOW
      WHETHER IT WILL REALLY PROCEED.NEXT TYPE 'G' AND IT WILL
      DEMAND THE VALUES OF a,b,&c. GIVE THE NECESSARY VALUES
      NOW AND IT WILL START EXECUTION.AT THE END OF EXECUTION
      FOR THE GIVEN SET OF VALUES OF a,b,c IT WILL AGAIN ASK
      YOU WHETHER IT WILL CONTINUE.YOU CAN TYPE 'G' ON THE
      TERMINAL AND CONTINUE EXECUTION AS BEFORE OR YOU CAN
      QUIT BY TYPING 'X' AFTER THE *-MARK.
-------------------------------------------------------------------------

ALPHA=90.0;BETA=90.0;GAMMA=120.0

********    VALUES OF "H","K" & "L" ARE GIVEN BELOW    ********

              H = -7 TO +7
              K = -3 TO +3
              L = -35 TO +35

*************************************************************************

IL(1)=-35
DO 1 I=1,70
IL(I+1)=IL(I)+1
IH(1)=-7
DO 2 J=1,14
IH(J+1)=IH(J)+1
IK(1)=-3
DO 3 K=1,6
IK(K+1)=IK(K)+1
```

```
*********** DATA INITIATION ENDS HERE ***************
      PRINT 40;PRINT 40;PRINT 40
   40 FORMAT(//30X,10('*******'))
   50 FORMAT(//17X,'DETERMINATION OF INTERPLANAR SPACING CORRESPONDING
     1 TO (H,K,L) VALUES FOR DIFFERENT IRON-ZINC ALLOYS')
      PRINT 52,ALPHA,BETA,GAMMA
   52 FORMAT(//11X,'ALPHA=',F4.1,10X,'BETA=',F4.1,10X,'GAMMA=',F5.1)
      PRINT 'WHAT SHALL BE DO?'
      TYPE 51
   51 FORMAT(1X,'GIVE THE VALUES OF a,b AND c')
      ACCEPT 53,A,B,C
      PRINT 53,A,B,C
   53 FORMAT(///35X,'a=',F6.3,20X,'b=',F6.3,20X,'c=',F6.3)
      PRINT 61;PRINT 54
   61 FORMAT(//2X,'H',3X,'K',4X,'L',27X,'VALUES OF "D" FOR A FIXED
     1 PAIR OF VALUES OF "H" & "K" FOR "L"=-35 TO +35')
   54 FORMAT(1X,'---',1X,'---','!',27X,23('~~~~'))

      *************** CALCULATION STARTS HERE ***************
      S11=(B*C*SIND(ALPHA))**2
      S22=(C*A*SIND(BETA))**2
      S33=(A*B*SIND(GAMMA))**2
      S12=A*B*(C**2)*(COSD(ALPHA)*COSD(BETA)-COSD(GAMMA))
      S13=C*A*(A**2)*(COSD(GAMMA)*COSD(BETA)-COSD(BETA))
      S23=A*C*(A**2)*(COSD(BETA)*COSD(GAMMA)-COSD(ALPHA))
      V=A*B*C*SQRT(1.0-(COSD(ALPHA)**2)-(COSD(BETA)**2)-(COSD(BETA)
     1**2)+(2.0*COSD(ALPHA)*COSD(BETA)*COSD(GAMMA)))
      DO 20 J=1,15
      DO 20 M=1,7
      DO 20 N=1,71
      D(J,M,N)=V/SQRT((S11*IH(J)**2)+(S22*IK(M)**2)+(S33*IL(N)**2)
     1+(2.0*S12*IH(J)*IK(M))+(2.0*S23*IK(M)*IL(N))+(2.0*S13*
     2IH(J)*IL(N)))
      CONTINUE
      ************ CALCULATION ENDS HERE ***************
      DO 21 J=1,15
      DO 21 M=1,7
      PRINT 101,(IH(J),IK(M),(D(J,M,N),N=1,15))
      PRINT 102,(D(J,M,N),N=16,60)
      PRINT 103,(D(J,M,N),N=61,71)
   21 CONTINUE
  101 FORMAT(/1X,I2,2X,I2,1X,'!',15F8.4)
  102 FORMAT(8X,'!',15F8.4)
  103 FORMAT(8X,'!',11F8.4)
      GO TO 10
      END
```

ME - 1981 - M - KEM - CHA